Spin-orbit-induced chirality of Andreev states in Josephson junctions

Andres A. Reynoso,[1] Gonzalo Usaj,[2,3] C. A. Balseiro,[2,3] D. Feinberg,[4] and M. Avignon[4]
[1]*ARC Centre for Engineered Quantum Systems, School of Physics, The University of Sydney, NSW 2006, Australia*
[2]*Centro Atómico Bariloche and Instituto Balseiro, Comisión Nacional de Energía Atómica (CNEA), 8400 Bariloche, Argentina*
[3]*Consejo Nacional de Investigaciones Científicas y Técnicas (CONICET), Argentina*
[4]*Institut Néel, CNRS and Université Joseph Fourier, 38042 Grenoble, France*
(Received 22 September 2012; published 28 December 2012)

We study Josephson junctions (JJs) in which the region between the two superconductors is a multichannel system with Rashba spin-orbit coupling (SOC) where a barrier or a quantum point contact (QPC) is present. These systems might present unconventional Josephson effects such as Josephson currents for zero phase difference or critical currents that *depend on* the current direction. Here, we discuss how the spin polarizing properties of the system in the normal state affect the spin characteristics of the Andreev bound states inside the junction. This results in a strong correlation between the spin of the Andreev states and the direction in which they transport Cooper pairs. While the current-phase relation for the JJ at zero magnetic field is qualitatively unchanged by SOC, in the presence of a weak magnetic field, a strongly anisotropic behavior and the mentioned anomalous Josephson effects follow. We show that the situation is not restricted to barriers based on constrictions such as QPCs and should generically arise if in the normal system the direction of the carrier's spin is linked to its direction of motion.

DOI: 10.1103/PhysRevB.86.214519 PACS number(s): 03.75.Lm, 71.70.Ej, 72.25.Dc, 74.45.+c

I. INTRODUCTION

The study of spin-orbit coupling (SOC) and related effects is one of the most active fields in mesoscopic physics. As the fabrication techniques improve, the link between the orbital and the spin degrees of freedom can be engineered allowing for the exploration of quantum phenomena at a deeper level.[1–4] Moreover, the importance of SOC goes far beyond mesoscopic device design as, for example, it has led to the identification of the quantum spin Hall phase in topological insulators,[5] a new phase of matter.[6,7] More recently, hybrid systems involving SOC and superconductivity have become one of the most investigated platforms.[8,9] When in combination with an appropriate magnetic field (generated externally or induced by proximity with a magnet in the sample), the system is expected to develop topological superconductivity.[10,11] This opens the possibility to synthesize Majorana fermions in semiconducting quantum wires, cold atoms, or devices based on topological insulators.

In this work, we theoretically investigate the dc Josephson effect in a hybrid system having superconductivity and spin-orbit coupling; more precisely, two *s*-wave superconducting leads (S) coupled by a two-dimensional normal region (N) that has Rashba spin-orbit coupling. For superconductor-normal-superconductor (S-N-S) junctions, it has been recognized that the interplay between external magnetic fields—or, alternatively, intrinsic magnetism—and the spin-orbit coupling can change the relation between the supercurrent and the phase difference between the two superconductors.[12–20]

The key ingredient in the S-N-S junction studied here is that the normal region *contains* a gate-voltage controlled barrier, see, for instance, the Josephson junction measured in Ref. 21. In Ref. 22, a weak external magnetic field, applied in a specific in-plane direction, was predicted to generate a controllable phase shift in the current-phase relation (CPR), i.e., the system develops a supercurrent for zero phase difference between the superconductors. As the gate voltage is reduced, and the barrier allows the transport of a few (more than one) transmission channels, the Josephson current becomes nonsymmetrical as a function of the phase. The maximum dissipationless current, the critical current, depends on the direction of the current and therefore there exists a current window on which the supercurrent is rectified.

In the long Josephson junction limit with transparent S-N interfaces, a normal region with a one-dimensional (1D) spin-orbit coupling combined with a magnetic field, either parallel or perpendicular to the SOC axis, can only produce transitions between 0-π junctions as it is the case for superconductor-ferromagnet-superconductor (S-F-S) junctions.[23,24] In this limit, this can be understood using Kulik theory,[25] but the same result follows by virtue of symmetry relations of the Bogoliubov-de Gennes (BdG) Hamiltonian,[26,27] irrespective of the geometry of the junction for any generic 1D SOC coupling. On the other hand, the magnetic field triggers shifts in the CPR by incorporating the mixing with other subbands in an effective 1D model.[13,14]

In the junction studied here, the anomalous effects arise because the barrier in the normal region [e.g. a two-dimensional electron gas (2DEG) in a semiconducting quantum well] behaves as an unconventional spin polarizer. As it was reported by Eto *et al.* in Ref. 28, a quantum point contact (or barrier) in a multichannel normal material with Rashba SOC spin polarizes the current without the need for magnetic fields or ferromagnets.[29–32] The larger the spin-orbit strength and the smoother the barrier, the more the polarization grows. Due to time-reversal symmetry, the favored spin projection reverses if the direction of the transport is inverted.

At zero magnetic field, we show how these gate-voltage controllable spin polarizing features in the normal device induce a correlation between the velocity[33] and the spin of Andreev states. As a result, the application of a magnetic field, along the direction in which the SOC polarizes the current, triggers the mentioned anomalous Josephson effects.

We present a simple WKB picture for the transport through the barrier that successfully explains the main features of the exact numerical results for the Andreev states including their spin texture. We also show that the anomalous Josephson effects are not restricted to QPCs, they also appear in wider barriers (stripe-shaped samples) for which the transverse modes are so close in energy that the plateaus of quantized conductance cannot be resolved when changing the gate voltage. For both types of barriers, N-S junctions with reduced transparency make the normal device behave as a Fabry-Perot interferometer;[34] the total transmission and the polarization are maximized at particular values of the gate voltage that controls the barrier. This resonant behavior translates into stronger Josephson anomalies that can be tuned by changing the gate voltage by a small amount.[22]

The paper is organized as follows: in Sec. II, we introduce the model and we outline the polarizing mechanism of the normal device, in Sec. III, we focus on how the spin properties of the Andreev states result in the anomalous Josephson effects mentioned above, and conclusions are presented in Sec. IV.

II. THE MODEL AND THE PROPERTIES OF THE NORMAL DEVICE

A. Model for the junction

Our model describes a Josephson junction with a QPC or barrier in a normal region that has spin-orbit coupling. The device, illustrated at the top of Fig. 1, includes two superconducting leads—left (L) and right (R)—and a central normal part (N) made out of a 2DEG in which the barrier is created with the help of electrostatic gates. For convenience, we assume that the three regions are restricted to a stripe geometry, i.e., the potential becomes infinite outside the region $0 < y < W_y$. The Hamiltonian describing the leads is

$$\hat{H}_\gamma = \int d\boldsymbol{r}\Bigg[\sum_\sigma \boldsymbol{\Psi}^\dagger_\sigma(\boldsymbol{r})\left(\frac{\boldsymbol{p}^2}{2m_s} - \mu\right)\boldsymbol{\Psi}_\sigma(\boldsymbol{r}) - \Delta_\gamma(\boldsymbol{r})\boldsymbol{\Psi}^\dagger_\uparrow(\boldsymbol{r})\boldsymbol{\Psi}^\dagger_\downarrow(\boldsymbol{r}) - \Delta^*_\gamma(\boldsymbol{r})\boldsymbol{\Psi}_\downarrow(\boldsymbol{r})\boldsymbol{\Psi}_\uparrow(\boldsymbol{r})\Bigg]. \quad (1)$$

Here, $\gamma = L,R$ and the integral is done in the $x < x_L$ semispace or the $x > x_R$ semispace for the left and right leads, respectively. In the above expression, m_s is the electron mass in the superconductor, μ is the chemical potential, and $\boldsymbol{\Psi}^\dagger_\sigma(\boldsymbol{r})$ creates an electron with spin σ at position $\boldsymbol{r} = (x,y)$. We assume that within the leads the superconducting order parameter is constant and set $\Delta_L(\boldsymbol{r}) = \Delta_0$ and $\Delta_R(\boldsymbol{r}) = \Delta_0 e^{i\phi}$. In the following, we take $\Delta_0 = 1.5$ meV as in Nb.

The normal part of the junction, $x_L < x < x_R$, is described by the Hamiltonian of a 2DEG with Rashba SOC and the potential $V(\boldsymbol{r})$ that defines the barrier:

$$\hat{H}_N = \int d\boldsymbol{r}\sum_{\sigma,\sigma'}\boldsymbol{\Psi}^\dagger_\sigma(\boldsymbol{r})\mathcal{H}_N\boldsymbol{\Psi}_{\sigma'}(\boldsymbol{r}),$$
$$\mathcal{H}_N = \frac{1}{2m^*}\left(p_x^2 + p_y^2\right) + \frac{\alpha}{\hbar}(p_y\sigma_x - p_x\sigma_y) + V(\boldsymbol{r}) - \mu\,, \quad (2)$$

where m^* is the effective mass of the 2DEG carriers, α is the strength of the Rashba coupling, and σ_i is the i component of the spin operator. The potential $V(\boldsymbol{r})$ includes a constant term that shifts the bottom of the conduction band of the 2DEG with respect to the one in the superconductor.

As in Ref. 22, we consider thin superconducting films parallel to the (x,y) plane. In this configuration, in-plane magnetic fields lead only to Zeeman interaction. Therefore the contribution to the Hamiltonian due to an external in-plane

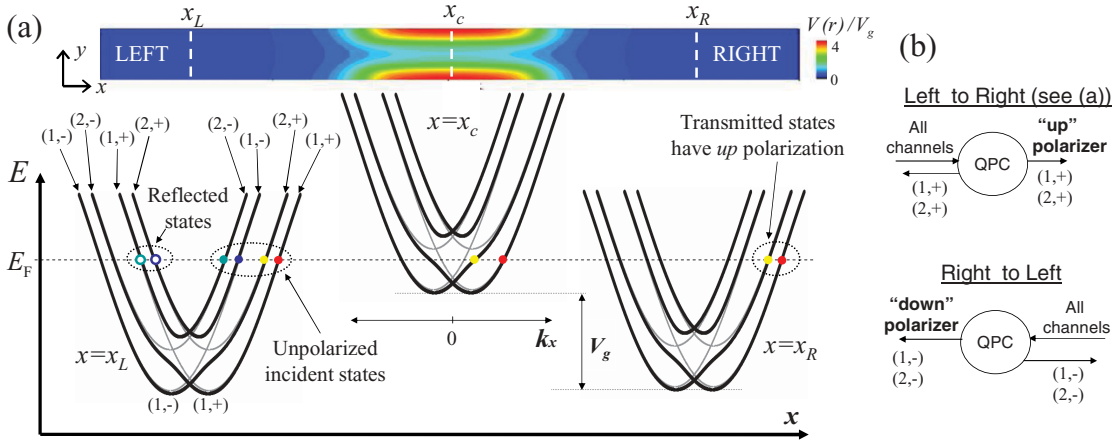

FIG. 1. (Color online) (a) Top: scheme of the junction including the leads and a qualitative color plot of the barrier potential $V(\boldsymbol{r})$; V_g is the value at the saddle-point. Bottom: qualitative two-mode picture of how the current through the barrier becomes spin polarized (left to right case). In the dispersion relations $E(k_x)$ at different positions, we indicate the relevant states using dots at the Fermi energy E_F. Electrons from the left lead (at $x = x_L$) are injected in four states, (n,σ_y), with $n = 1,2$ and $\sigma_y = \pm$. The barrier allows only one transverse mode to be transmitted (first conductance plateau, $G = 2e^2/h$). Electrons injected at $x = x_L$ in states $(1,+)$ and $(2,+)$ are transmitted to the right. They arrive at $x = x_R$ in states $(1,+)$ and $(2,+)$ and therefore the current is up polarized along y direction. Notice that—in the passage through the barrier—an electron injected in state $(1,+)$ does not see any avoided crossing (as in a zero-SOC barrier), whereas an electron injected in state $(2,+)$ suffers two SOC-induced avoided crossings: first it is mixed with $(1,-)$ and then it returns to $(2,+)$. (b) Summary of the left to right and right to left transport properties of the barrier. The spin polarization from right to left is $down$ as electrons injected (at $x = x_R$ from the right lead) in $(1,-)$ and $(2,-)$ are transmitted whereas electrons injected in $(1,+)$ and $(2,+)$ are reflected to $(2,-)$ and $(1,-)$, respectively.

magnetic field is

$$\hat{H}_Z = \int d\boldsymbol{r} \sum_{\sigma,\sigma'} \boldsymbol{\Psi}^\dagger_\sigma(\boldsymbol{r}) \frac{g(x)\mu_B}{2} (B_x\sigma_x + B_y\sigma_y)\boldsymbol{\Psi}_{\sigma'}(\boldsymbol{r}), \quad (3)$$

where B_i are the components of the magnetic field and the gyromagnetic factor,

$$g(x) = \begin{cases} g_N, & \text{for} \quad x_L < x < x_R, \\ g_S, & \text{otherwise}, \end{cases} \quad (4)$$

is different for the leads and the normal region. In the regime of parameters studied in this paper, the superconducting contacts are almost unaffected by the magnetic field. Namely, we take the Zeeman energy E_Z on the normal region, always smaller than 20% of the superconducting gap Δ_0 in the S contacts. As the g factor in the In-based 2DEG is at least five times larger that the g factor in the superconductor, the Zeeman energy in the superconductor is at most $\Delta_0/25$.

In the present work, we solve the full Hamiltonian, $\hat{H} = \hat{H}_Z + \hat{H}_N + \hat{H}_L + \hat{H}_R$, numerically using a finite difference approach.[35] This is done by writing a tight-binding version of the Hamiltonian and using a recursive Green function method.[36] The details of the approach are presented in Appendix. For $\Delta_0 \neq 0$, one must work in a Nambu space representation since $\hat{H}_{\text{tot}}$ is indeed a BdG Hamiltonian.[37]

In the lattice model, the tunneling between the normal and superconducting materials is described by hopping Hamiltonians, $\hat{H}_{N,L}$ and $\hat{H}_{N,R}$. The sites at the interfaces are connected by a spin-conserving matrix element t_b that arises due to the kinetic term in the original Hamiltonian ($\propto p_x^2$). As shown in Eq. (A7), there are also spin-flipping tunneling elements between those sites. These arise due to the symmetrization made to assure Hermiticity of the SOC term:[38]

$$-\frac{\alpha(x)}{\hbar} p_x\sigma_y \to -\frac{1}{2\hbar}[\alpha(x)p_x + p_x\alpha(x)]\sigma_y. \quad (5)$$

Clearly, such symmetrization is relevant only where $\partial_x\alpha(x) \neq 0$; here, the interfaces between the normal region and the superconductors.

As assumed in the classic Blonder-Tinkham-Klapwijk (BTK) approach for studying Andreev reflection,[39] nonideal transparencies can be introduced through a sharp potential at the N-S interfaces in the continuous model. In the lattice model, the transparency of the barrier is controlled by the parameter A such that

$$t_b = A\,\frac{t_N + t_S}{2}, \quad (6)$$

where t_S and t_N are the hopping parameters for the superconducting and normal regions, respectively. Notice that for realistic junctions, t_S and t_N are different since they are chosen to simulate the Fermi velocity and electron mass mismatches between the 2DEG and the superconductor. A transparent junction corresponds to $A = 1$ since in such a case, t_b is the average of the hopping in the two regions minimizing the scattering at the S-N interfaces; choosing $A < 1$ allows for the simulation of poorer transparencies. To achieve the full transparent junction case ($Z = 0$ case of BTK), it is not enough to set $A = 1$ but we also need to assume that $t_S = t_N$. Besides the interface parameter A, the junction is characterized geometrically by its total length, $L_N = x_R - x_L$, by the properties of the barrier (see Appendix) and by the number of transverse channels in the normal region.

B. Normal device: Spin polarization due to a barrier potential

Understanding normal transport through smooth barriers in presence of spin-orbit coupling is a prerequisite to the investigation of the JJs we treat here. Therefore, in this section, we focus on the case in which the leads are not superconducting but instead they are a continuation of the normal region (case I) or a metallic material M, different from the spin-orbit coupled 2DEG in the central region (case II). For the case I, Eto *et al.*[28] have shown that a 2DEG with a QPC is able to spin-polarize the current without the help of an external Zeeman field. They assume a Rashba SOC and study the ballistic transport through QPCs described by a quite general saddlelike potential.

1. Origin of the current polarization: A qualitative picture

We focus on case I for which the interfaces 2DEG-leads do not introduce backscattering. The main underlying mechanism can be exemplified using two conducting channels $n = 1,2$ in a Wentzel-Kramers-Brillouin (WKB) picture.[40] At every position x_a, one obtains the dispersion relation that would follow if the system were infinitely long with the y-dependent potential, $\widetilde{V}_{x_a}(y) \equiv V(x_a, y)$. We first exclude from the Hamiltonian of the normal region in Eq. (2) the part of the Rashba SOC proportional to the perpendicular momentum, $\mathcal{H}^{\text{so}}_\perp = \frac{\alpha}{\hbar} p_y\sigma_x$. For $\mathcal{H}^{\parallel} \equiv \frac{\mathbf{p}^2}{2m^*} - \frac{\alpha}{\hbar} p_x\sigma_y + \widetilde{V}_{x_a}(y)$, solutions at x_a are uniquely identified by k_x, by the spin projection along the y axis, $\sigma_y = \pm$, and by the transverse mode number n. For each transmission channel, (n,σ_y), the k_x solution at position x_a is $|\Phi_{x_a,n}\rangle|k_x\rangle|\sigma_y\rangle$, with eigenenergies:

$$E^{\parallel}_{(n,\sigma_y)}(x_a) = \frac{\hbar}{2m^*}(k_x - k_\alpha\sigma_y)^2 - E_\alpha + E^V_n(x_a), \quad (7)$$

where $k_\alpha \equiv \frac{m^*\alpha}{\hbar^2}$, $E_\alpha \equiv \frac{\hbar^2 k_\alpha^2}{2m^*} = \frac{\alpha^2 m^*}{2\hbar^2}$, and $E^V_n(x_a)$ are the transverse mode energies, namely, the eigenenergies corresponding to the eigenfunctions, $\langle y|\Phi_{x_a,n}\rangle$, of the Hamiltonian $\frac{p_y^2}{2m^*} + \widetilde{V}_{x_a}(y)$.

Importantly, the $E^{\parallel}_{(n,\sigma_y)}(x_a)$ parabolas for modes $(1,-)$ and $(2,+)$ [as well as for $(1,+)$ and $(2,-)$] cross each other; see gray lines in Fig. 1(a). Away from the center of the barrier and for strong enough Rashba interaction these crossings are *below* the Fermi level E_F. The transverse SOC, $\mathcal{H}^{\text{so}}_\perp \propto p_y\sigma_x$, produces avoided crossings because it coherently mixes transverse modes with different parity, n mod 2, (since $p_y = -i\hbar\frac{\partial}{\partial y}$) and opposite σ_y. Figure 1(a) sketches the transport through the QPC in the adiabatic picture. For the situation shown there, the value of the potential at the saddle point V_g is tuned to allow the passage of a single transverse mode: the conductance is $2e^2/h$. As electrons at E_F pass through the QPC from left to right their k_x momentum change. Electrons in the lowest-lying split channel $(1,+)$ pass through unaffected. On the other hand, electrons in the higher split channel $(2,+)$ are swept twice through the anticrossing: first changing to $(1,-)$ and then to $(2,+)$. Incoming electrons occupying the *down* modes $(1,-)$ and $(2,-)$ (see contact with the left lead at position x_L) do not arrive at x_c (center of the barrier) but instead they are backscattered to x_L into the left-traveling modes $(2,+)$

and (1,+), respectively. Thus the current arriving at x_R (the position of the contact with the Right lead) is up-spin polarized along the y direction.

In the two-modes sketch of Fig. 1, we have assumed that the avoided crossings are fully effective. In a more general case, the two quantum channels associated to the first transverse mode can be divided in (i) channel (1,+), which is fully transmitted to x_R without state conversion, and (ii) combination of (2,+) and (1,−) that arrives to x_R after mixing in region of the barrier. The larger the strength of the Rashba coupling and/or the smoother the barrier potential, the more effective are the avoided crossings and the better becomes the polarizer: the contribution to the current of the (2,+) quantum channel is increased. As the polarization is defined by the transport properties of electrons at the Fermi level, what matters most is the gradient of the barrier potential at the positions $x^{\rm ac}$ in which the crossings between the relevant dispersions fall at $E_{\rm F}$, i.e.,

$$E_{\rm F} = E^{\parallel}_{(1,\sigma_y)}(x^{\rm ac}) = E^{\parallel}_{(2,\bar{\sigma}_y)}(x^{\rm ac}). \tag{8}$$

Two positions, $x_L^{\rm ac} < x_c$ and $x_R^{\rm ac} > x_c$, fulfill this condition. If the barrier is symmetric with respect to x_c, both avoided crossings share the same effectiveness. In Ref. 28, the probability of state conversion is estimated—using the Landau-Zener formula for the case that $\widetilde{V}_x(y)$ is a hard-wall constriction potential of variable width $W(x)$—as $p_{L,R} = 1 - {\rm e}^{-2\pi\lambda}$ with $\lambda \approx k_\alpha |W(x_R^{\rm ac})/[\frac{dW}{dx}(x_{L,R}^{\rm ac})]|$.

Notice that for barriers with coexistence of Rashba and Dresselhaus SOCs, nonzero polarization arises in exactly the same way along the direction of the spin operator that multiplies p_θ, with $\hat{\theta} \equiv (\cos\theta, \sin\theta)$, the direction parallel to the current that flows through the barrier (here, $\hat{\theta} = \hat{x}$ and the corresponding spin operator for the Rashba SOC is σ_y). This opens the possibility to electrically change the spin-polarization axis of an Eto *et al.* polarizer as the Rashba strength is tuned with gate voltage[41] and the Dresselhaus interaction remains constant.

2. *Time-reversal symmetry and transport from right to left*

In the above discussion, we have focused on the left (L) to right (R) transport in the symmetric case. We now relax the condition of spatial symmetry of the barrier profile allowing it to be different for $x < x_c$ and for $x > x_c$. Therefore we assume that the probability to follow the avoided crossing is p_L at $x_L^{\rm ac}$ and p_R at $x_R^{\rm ac}$. For the two-channel model, with the barrier in the first plateau of conductance, the nonzero transmission coefficients (from left to right) at the Fermi energy are

$$T_{(L,1,+)\to(R,1,+)} = 1, \tag{9a}$$
$$T_{(L,1,-)\to(R,1,-)} = (1-p_L)(1-p_R), \tag{9b}$$
$$T_{(L,1,-)\to(R,2,+)} = (1-p_L)p_R, \tag{9c}$$
$$T_{(L,2,+)\to(R,1,-)} = p_L(1-p_R), \tag{9d}$$
$$T_{(L,2,+)\to(R,2,+)} = p_L p_R. \tag{9e}$$

The conductance G, the polarization of the transmitted electrons P, and the relative spin polarization of the incoming electrons that contribute to the current D, can be expressed in terms of the transmission coefficients as

$$G_{L\to R} = \frac{e^2}{h} \sum_{n_L,\sigma_{y,L}} \sum_{n_R,\sigma_{y,R}} T_{(L,n_L,\sigma_{y,L})\to(R,n_R,\sigma_{y,r})}, \tag{10a}$$

$$P_{L\to R} = \frac{e^2}{hG} \sum_{n_L,\sigma_{y,L}} \sum_{n_R,\sigma_{y,R}} \sigma_{y,R} T_{(L,n_L,\sigma_{y,L})\to(R,n_R,\sigma_{y,R})}, \tag{10b}$$

$$D_{L\to R} = \frac{e^2}{hG} \sum_{n_L,\sigma_{y,L}} \sum_{n_R,\sigma_{y,R}} \sigma_{y,L} T_{(L,n_L,\sigma_{y,L})\to(R,n_R,\sigma_{y,R})}, \tag{10c}$$

where the subscript $L \to R$ refers to the left to right transport. For the polarizing barrier, we introduce the coefficients of Eq. (9) in Eq. (10) obtaining $G_{L\to R} = \frac{2e^2}{h}$, $P_{L\to R} = p_R$ and $D_{L\to R} = p_L$.

Importantly, due to time-reversal symmetry, the resolved transmission coefficients at the Fermi energy fulfill the following relation:

$$T_{(L,n_L,\sigma_L)\to(R,n_R,\sigma_R)} = T_{(R,n_R,\bar{\sigma}_R)\to(L,n_L,\bar{\sigma}_L)}. \tag{11}$$

Therefore the resolved transmission in the opposite direction of electrons with opposite spins (at both ends) is identical. This follows from the self-duality of the scattering matrix in a spin-1/2 time-reversal symmetric system.[42] Here, this expression is of great importance for the Josephson effect because at the S-N interfaces an electron coming from the normal region can be Andreev-reflected back to the normal as the lack of an electron with opposite spin (a hole) in the same transverse mode. Since this hole propagates as the lacking electron, Eq. (11) establishes the main difference with a conventional magnetism-based polarizer. In the latter systems, irrespective of the direction of the current, the largest transmission is for electrons with spins parallel to the majority spin.

For the polarizing barrier treated here, by combining the time reversal relation with Eqs. (9) and (10), we get that the normal transport from right to left has $G_{R\to L} = \frac{2e^2}{h}$, $P_{R\to L} = -p_L$, and $D_{R\to L} = -p_R$. Note that for the case of the smooth symmetrical barrier with strong Rashba of Fig. 1, $p_L = p_R \approx 1$ and thus $P_{R\to L} = -P_{L\to R} \approx 1$. The inversion of the sign of the polarization is summarized in Fig. 1(b). It can also be understood from the WKB picture in Fig. 1(a) by noting that the electrons arriving to L are due to incoming electrons from R entering the sample: (i) in channel (1,−) passing through the barrier without mixing or (ii) in channel (2,−) arriving to L in channel (2,−) after mixing in the region of the barrier with channel (1,+).

We have introduced the two most important differences between the Eto *et al.* polarizer and a magnetism-based spin polarizer. First, here the device polarizes even though the conductance is equivalent to two quantum channels, this contradicts the naive expectation that $G = 2e^2/h$ implies spin degeneracy and that therefore the polarization should be zero. The second distinctive feature is that in symmetrical barriers the spin polarization of the transmitted current reverses when the current flow is reversed. More generally, irrespective of the spatial symmetry of the barrier, we have that $P_{L\to R} = -D_{R\to L}$ and $P_{R\to L} = -D_{L\to R}$, which means that the SOC induced polarization does not conspire against the formation of Andreev states. The preferred spin direction for the transmitted

electrons arriving to a given N-S interface is exactly opposite to the preferred spin direction for the incoming electrons (or lack of them) that can be transmitted to the other side of the barrier. In Sec. III, we study which properties of Andreev states are affected when these SOC-based polarizer barriers are present inside a S-N-S Josephson junction and how these properties manifest when a weak Zeeman energy is present.

3. *Numerical results in more realistic models*

Using the QPC potential of Eq. (A1) and the tight-binding model, we compute the conductance and the polarization in devices with many channels. In Fig. 2, results are presented as a function of V_g for cases I and II described above. We have chosen the opposite limit to the one shown in Fig. 1: the SOC strength is weak, the avoided crossings are not fully effective and thus the polarization is not strong. Case I is shown in Fig. 2(a), as the leads are 2DEG based, the scattering back to the barrier is minimized and the plateaux of conductance are well defined. The SOC-induced current polarization is always smaller than 5%, the characteristic value in the first plateau is $P^{1st}_{(I)} = 0.04$.

Figure 2(b) shows results for the case II in which the leads are metals and therefore the electrons at the 2DEG-M interfaces are strongly scattered back to the 2DEG region. Resonances in the conductance are observed for special values of V_g. Correlatively, the spin polarization of the current shows maxima too. Notice that the average spacing between these maxima is larger than that of the conductance maxima. The main result is that constructive interferences, due to multiple

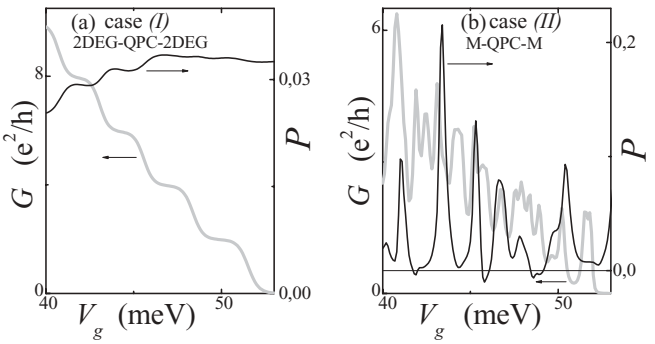

FIG. 2. Conductance G (gray line) and polarization P (black line) as a function of V_g for the quantum point contact QPC_2 described by Eq. (A1) taking $(z; W_b; L_b) = (90; 100; 250)$ nm. The 2DEG parameters are for an InAs-based 2DEG, ($n = 10^{12}$ cm^{-2} and $m^* = 0.045m_e$ with m_e the electron mass) $E_F = 53.3$ meV, $\alpha = 5$ meVnm, and $L_N = x_R - x_L = 1.2$ μm. In the simulation, we take $W_y = 180$ nm and $a_0 = 3$ nm. (a) Case I, 2DEG-QPC-2DEG: the leads are the same 2DEG and therefore the scattering at the interfaces is absent. As the Rashba strength is weak the polarization is small: less than 4% in the first plateau. (b) Case II, M-QPC-M : the leads are a metallic material M different from the 2DEG leading to a strong backscattering at the M-2DEG junctions; taking metallic Nb as a reference we use $m^*/m_s = 0.045$ and the Fermi velocities ratio, $v_F^{2DEG}/v_F^{Nb} \approx 2.25$. Due to Fabry-Perot interference-like effects, both the conductance and the polarization show resonant behavior as a function of V_g; remarkably, there are values of V_g in which the polarization can be much larger than the sub 4% values observed when the device is in between 2DEG leads.

reflections of channels between the interfaces and the QPC, strongly boost the current spin polarization with respect to case I. We have checked (not shown) that the relative polarization enhancement, $P^{peak}_{II}/P^{1st}_{I}$, grows the weaker is the SOC strength. It is interesting to analyze this amplification mechanism for the same phenomenon is correlated with the anomalous Josephson current amplitude in the S-QPC-S case.

A simplified scattering theory is sufficient for a qualitative understanding.[34] It includes the two lowest channels, the M-2DEG interfaces with a reflection coefficient r_0, the SOC strength through the probability p of state conversion at the avoided crossing between channels $(1,\sigma_y)$ and $(2,\bar{\sigma}_y)$, and the phases accumulated through the QPC for each of the quantum channels. These phases can be calculated by a WKB formula, they depend both on the junction length and on the gate voltage. The result of this calculation is that the full transmission (thus the conductance) as well as the spin polarization oscillate with the accumulated phases due to Fabry-Perot interferometry-like effects. As in the exact full numerical simulation presented in Fig. 2 for a much larger total number of channels, taking a large r_0 value, one sees: (i) the ratio between the polarization value at the peaks and the polarization for $r_0 = 0$ is larger the weaker is the Rashba strength and (ii) the oscillation period for the polarization is larger than the one of the conductance. The explanation for this is that the spin polarization of the current crucially depends on a coherent mixing of split channels with opposite spin directions. The polarization is controlled by the phase accumulated in the region *between* the output interface, at x_R, and the closest mixing location, at x_R^{ac}. On the other hand, the full transmission is sensitive to the phase acquired through the whole length of the device, thus explaining the faster variation of the conductance with the gate voltage.[34]

III. THE EFFECT OF SOC-BASED POLARIZERS IN JOSEPHSON JUNCTIONS

Defining the superconducting phase difference, $\phi \equiv \phi_L - \phi_R$, the Josephson current is given by[37,43]

$$I = \frac{2e}{\hbar}\left\langle \frac{\partial \hat{H}}{\partial \phi} \right\rangle = \frac{2e}{\hbar}\int_{-\infty}^{\infty} J(\varepsilon,\phi) f_0(\varepsilon)\, d\varepsilon, \qquad (12)$$

where $\langle \cdots \rangle$ indicates the expectation value at thermal equilibrium, $f_0(x) = 1/(1 + e^{x/k_B T})$ is the Fermi distribution and we have introduced the Josephson current density

$$J(\varepsilon,\phi) = \sum_j \frac{\partial \varepsilon_j}{\partial \phi}\, \delta[\varepsilon - \varepsilon_j(\phi)]\,. \qquad (13)$$

Thus $J(\varepsilon,\phi)$ contains the information about the velocity at which Cooper pairs (i.e., charge $2e$) are transmitted via Andreev bound states, namely, the states with energy ε_j, which have nonzero $\frac{1}{\hbar}\frac{\partial \varepsilon_j}{\partial \phi}$. As we discuss below, the eigenvalues ε_j of the system do not need to be computed in order to get the Andreev levels. It is sufficient to compute $J(\varepsilon,\phi)$ and later identify the coordinates (ε,ϕ) at which $J(\varepsilon,\phi)$ contributes to the current. In the discretized model presented in Appendix, the current is obtained from Eq. (A11). The calculation involves expectation values that can be expressed as integrals over ε of retarded and advanced Green function.[44] This method

allows us to directly obtain $J(\varepsilon,\phi)$ and from it identify the contributing Andreev energy levels.

Notice that in the regime of parameters we work, 4π-periodic components are not present as the magnetic field is weak and it is applied *parallel* to the direction of the SOC field; this is not the regime appropriate for Majorana physics.[11,45] Here, due to the SOC-polarizing barriers and by virtue of a small magnetic field along the polarization direction, we find strongly asymmetric (2π-periodic) $I(\phi)$ shapes. We have verified that the shapes always fulfill

$$\int_0^{2\pi} I(\phi)d\phi = \frac{2e}{\hbar}(\langle\hat{H}\rangle_{\phi=2\pi} - \langle\hat{H}\rangle_{\phi=0}) = 0\,, \qquad (14)$$

i.e., the area below the CPR is zero. This trivial property is not evident from the plots reported in the following sections.

A. Anomalous Josephson effects enhanced by barriers with SOC: Ideal interfaces

In this section, we study the case of ideal S-N interfaces in order to isolate the effect in the Josephson current due to the presence of SOC-induced spin polarization—in Sec. III B, we will focus on how the basic properties discussed here are modified by the resonant-like behavior that appears for more realistic interfaces.[22] The effective mass and Fermi velocity of the superconducting leads are matched to the ones of the 2DEG and normal reflection (for $|\varepsilon| < \Delta_0$) is minimized. In the lattice model, this is achieved by setting $t_S = t_N = t_b$ [$A = 1$ in Eq. (6)].

1. *Spin properties of Andreev states in absence of magnetic field*

Figure 3 shows the results for zero magnetic field for a device with strong SO coupling. In Fig. 3(a), we show a map of the local density of states (LDOS) at $x = x_R$ as a function of ε and ϕ: $\rho_{X_R}(\varepsilon,\phi)$ (see Appendix). The nondispersive states are due to modes that are reflected at the barrier and do not contribute to the Josephson current density shown in Fig. 3(b). For the gate-voltage shown, the barrier allows the transmission of a single transverse mode. Thus, at each side of the barrier, there are standing waves that can not transport Cooper pairs from one superconductor to the other—except for an exponentially small contribution due to quantum tunneling.

On the other hand, the Andreev bound states—those contributing to the current—have an apparent linear behavior with ϕ. The sign of their contributions to $J(\varepsilon,\phi)$ is correlated with the sign of their slopes: the latter are linked to the *velocity* of the Andreev states [cf. Eq. (13), see Fig. 3(b)]. In Fig. 3(c), we present the total Josephson current I, which is given by the integral in Eq. (12). It includes the contributions of both the discrete (Andreev bound states) and of the continuum ($|\varepsilon| > \Delta_0$) spectrum. The most important contribution comes from the Andreev bound states.[39,46] The shape of the CPR for zero field does not show signatures of the presence of the SOC and the barrier: similar triangular-like CPR shapes are expected in S-N-S long junctions with high transparency at the S-N interfaces.[21,25,47–49]

Even though the magnetic field is zero, the Andreev levels are not spin degenerate [see Fig. 3(d)]. This is due to the Rashba coupling in the normal region and—as it becomes clearer below—the effect is enhanced by the presence of the

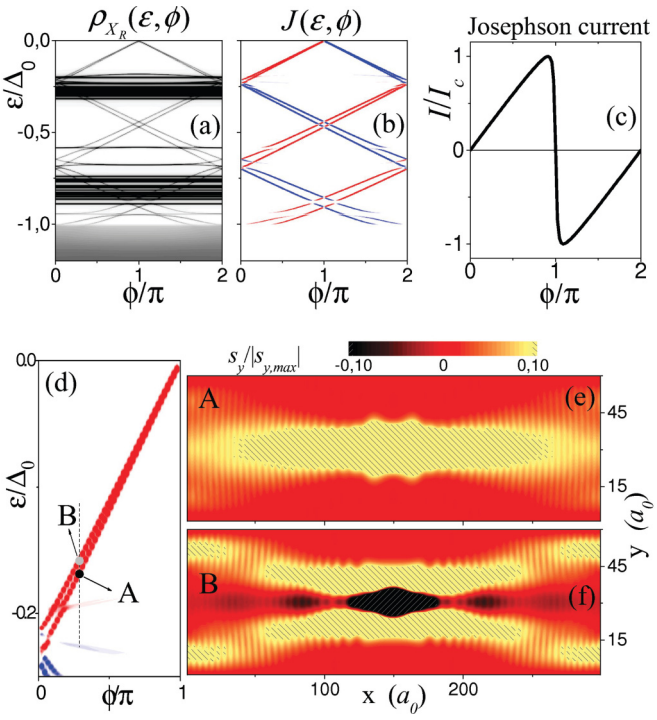

FIG. 3. (Color online) Exact results for the full multichannel model of a Josephson junction with a SOC-based spin-polarizing barrier. The superconductors have $\Delta_0 = 1.5$ meV and are chosen to minimize normal reflection (see text). The normal region length is $L_N = 300a_0 = 900$ nm and the QPC parameters are those given in Fig. 2. Here, the gate voltage is set in the middle of the first conductance plateau and the SOC is strong, $\alpha = 40$ meVnm, so that the polarization is close to one. Color maps as a function of energy ε and the superconducting phase difference ϕ for (a) $\rho_{X_R}(\varepsilon,\phi)$, the local density of states at the last layer of the normal, X_R; (b) and (d) $J(\varepsilon,\phi)$, the current density. Notice that $J(\varepsilon,\phi)$, for $|\varepsilon| < \Delta_0$, images the Andreev states; those that contribute to the current (red and blue—in the online version—are positive and negative contributions, respectively, given by the sign of the slope $\frac{\partial\varepsilon_j}{\partial\phi}$). (c) Total Josephson current I, i.e., the integral of $J(\varepsilon,\phi)$. (e) and (f) Magnetization $s_y(x,y) = \frac{\hbar}{2}\langle\sigma_y\rangle$ at $\phi_a = 0.3\pi$ for Andreev states $|A\rangle$ and $|B\rangle$ [see (d) and the discussion in Fig. 4]. The magnetizations, integrated over all the normal sample, are positive: $s_y^B = 0.45 s_y^A$.

spin polarizer barrier. Let us fix $\phi = 0.3\pi$ and investigate the features of two neighbors Andreev states, $|A\rangle$ and $|B\rangle$. Notice that both Andreev levels have the same slope sign and therefore they transport Cooper pairs in the same direction. In a system without magnetism and without SOC, the two states $|A\rangle$ and $|B\rangle$ would be degenerate and their spin properties would be opposite to each other. Here the situation is different: the two Andreev states neither share the same transversal profile nor their spin properties are opposite; in Figs. 3(e) and 3(f), we show their spin density along the y direction—the direction in which the barrier polarizes the current as a result of the Rashba coupling.

In order to qualitatively analyze the results it is useful to resort to the WKB picture presented in Sec. II B. First, we notice that in the states $|A\rangle$ and $|B\rangle$ the Cooper pairs are transferred from the left (L) superconductor to right (R) superconductor (positive slope). Thus each Andreev bound

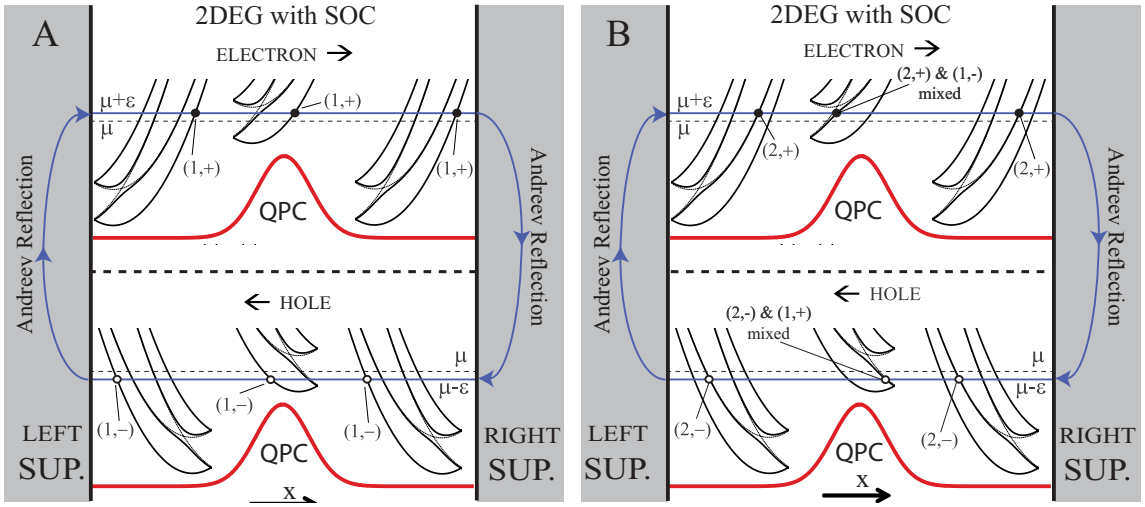

FIG. 4. (Color online) Sketch for the WKB interpretation of the Andreev states $|A\rangle$ and $|B\rangle$ shown in Figs. 3(d)–3(f). Both states have positive velocity, they transfer Cooper pairs from the left (L) to the right (R) superconductor. Figure 3 shows that the state $|A\rangle$ transports Cooper pairs at a faster rate (since $\frac{\partial\varepsilon_A}{\partial\phi} > \frac{\partial\varepsilon_B}{\partial\phi}$) and its s_y profile is always positive with a single maximum along the y direction, whereas s_y for the Andreev state $|B\rangle$ shows two positive maxima except from the center of the barrier where there exists a negative contribution to s_y having a *single* maximum. This is in full agreement with the WKB picture presented here. For the state $|A\rangle$ (left), the electron occupies the $(1,+)$ transverse mode all along the barrier as much as the reflected hole occupies the $(1,-)$ transverse mode. On the other hand for $|B\rangle$ (right), because of the smoothness of the barrier and the avoided crossings presented in Fig. 1, the electron (hole) is on the $(2,+)$ [$(2,-)$] mode away from the barrier and it mixes with the $(1,-)$ [$(1,+)$] close to the barrier. This explains the different patterns of local magnetization along the y direction, and why the Andreev state $|B\rangle$ is *slower* than the $|A\rangle$ one.

state is a stationary cyclic sequence of (i) electron traveling from L to R, (ii) electron-to-hole Andreev reflection at R, (iii) hole traveling from R to L, and (iv) hole-to-electron Andreev reflection at L.

For the subgap Andreev transport ($|\varepsilon| < \Delta_0$), we sketch in Fig. 4, two different possibilities left open by the device as V_g is tuned to allow a single transverse mode to transmit. The left panel shows different processes that lead to the state $|A\rangle$: the electron travels from L to R in the $(1,+)$ mode and it is Andreev reflected as the lack of an electron in the $(1,-)$ channel; then, this hole is transmitted in the $(1,-)$ channel from R to L where it is Andreev reflected as an electron back in channel $(1,+)$ and the loop closes. This is therefore an state with an overall spin-up polarization in the y direction and a transverse spatial profile given by the first transverse mode (which has a single maximum in the transverse direction). This is in agreement with the exact results for the spin profile shown in Fig. 3(e).

Similarly, the right panel of Fig. 4 focuses on the case of the Andreev state $|B\rangle$; the electron in its travel from L to R starts at mode $(2,+)$, it mixes with the $(1,-)$ mode in the region of the barrier and then arrives at R in the $(2,+)$ mode. It is Andreev reflected as the lack of an electron in $(2,-)$, this hole is transmitted arriving at L in $(2,-)$ but in the region of the barrier, it mixes with mode $(1,+)$. This is also in agreement with the exact quantum result shown in Fig. 3(f) for state $|B\rangle$, as the local spin density shows two positive maxima (spin *up* and second transverse mode) away from the barrier and a contribution with a single negative maximum (spin *down* and first transverse mode) appear in the region of the barrier. Furthermore, within this picture, it is also justified that the Andreev state $|A\rangle$ transports Cooper pairs at a faster rate than $|B\rangle$ [see greater slope with ϕ in Fig. 3 (d)] because in the first one, both electrons and holes are transmitted fully in the first transverse mode, which is at all positions faster than the other channels, as it is evident from the slopes $|\frac{dE}{dk}|$ in Fig. 1.

2. *Symmetry considerations and the weak magnetic field limit*

We start studying the symmetry properties of the BdG Hamiltonian $H_{\rm BdG}$ in absence of ferromagnetic materials and magnetic fields. In this case, we have

$$H_{\rm BdG}(-\phi) = \mathcal{T}^{-1} H_{\rm BdG}(\phi)\mathcal{T}, \tag{15}$$

where $\mathcal{T}$ is the time-reversal operator Notice that $-\phi$ is equivalent to $2\pi - \phi$. With the exceptions of $\phi = 0$ and $\phi = \pi$, Eq. (15) does not imply the existence of degenerate solutions for $H_{\rm BdG}$ at a fixed ϕ. Instead, it allows us to construct solutions for the case of $\phi = (2\pi - \phi_x)$ from the ones at $\phi = \phi_x$. Thus, for any given eigenstate (labeled by the natural number $j = 1,2,\ldots$) $|j\rangle$ at $(\varepsilon,\phi) = (\varepsilon_j,\phi_x)$, we know that

$$\begin{matrix} |j\rangle \\ (\varepsilon_j,\phi_x) \end{matrix} \Rightarrow \begin{matrix} |\bar{j}\rangle \equiv \mathcal{T}^{-1}|j\rangle \\ (\varepsilon_j, 2\pi - \phi_x) \end{matrix}. \tag{16}$$

This means that if the energy of $|j\rangle$ at $\phi = \delta\phi + \phi_x$ is given by $\varepsilon_j(\delta\phi) = \varepsilon_j(\phi_x) + b_j\,\delta\phi$, then the energy of $|\bar{j}\rangle$ at $\phi = \delta\phi + (2\pi - \phi_x)$ is $\varepsilon_{\bar{j}}(\delta\phi) = \varepsilon_j(\phi_x) - b_j\,\delta\phi$, with b_j the slope of the Andreev level for $|j\rangle$ at $\phi = \phi_x$. Therefore their velocities, v_j and $v_{\bar{j}}$, become opposite to each other ($v_j = -v_{\bar{j}}$) as they are proportional to $\frac{\partial\varepsilon_j}{\partial\phi}$ and $\frac{\partial\varepsilon_{\bar{j}}}{\partial\phi}$, respectively. This implies that the Josephson current must be zero for either $\phi_x = 0$ or $\phi = \pi$, as the two $\mathcal{T}$-related states share the same coordinates (ε,ϕ) so their individual contributions cancel out. For arbitrary values of ϕ, the following relations hold:

$$I(\phi) = -I(-\phi) = -I(2\pi - \phi), \tag{17a}$$

$$I(\pi + \phi) = -I(\pi - \phi). \tag{17b}$$

An obvious property implied by Eq. (17) is that the absolute value of the critical current is independent on the direction of the current, i.e., $I_c^+ = I_c^-$ with

$$I_c^+ \equiv \max I(\phi), \quad I_c^- \equiv |\min I(\phi)|. \tag{18}$$

In the next sections, we discuss how the barrier presented in Sec. II B provides a controllable way to violate the relation $I_c^+ = I_c^-$. In this section, we discuss the fate of the properties Eq. (17) when Eq. (15) no longer holds due to the presence of external magnetic fields coexisting with spin-orbit coupling.

Starting from the zero magnetic field condition, we group the Andreev states in $\mathcal{T}$-related states, $|j\rangle$ and $|\bar{j}\rangle$, and address the response of the energy levels to a weak external magnetic field. As $|\bar{j}\rangle$ is the time-reversed state of $|j\rangle$, they have opposite local spin projections,

$$\langle \boldsymbol{s}_j(\boldsymbol{r})\rangle \equiv \langle j|\boldsymbol{s}(\boldsymbol{r})|j\rangle = -\langle \bar{j}|\boldsymbol{s}(\boldsymbol{r})|\bar{j}\rangle = -\langle \boldsymbol{s}_{\bar{j}}(\boldsymbol{r})\rangle\,, \tag{19}$$

with $\boldsymbol{s} = \frac{\hbar}{2}\boldsymbol{\sigma}$ and $\boldsymbol{\sigma} = (\sigma_x,\sigma_y,\sigma_z)$. Let us assume, as an example, that the spin of the Andreev state $|j\rangle$ is *up* along the y-direction—then we know that $|\bar{j}\rangle$ is a *down* state. Thus, if a Zeeman field is applied along the y direction—provided it is not too strong to affect the properties of the original states—the energy levels corresponding to $|j\rangle$ (at $\phi = \phi_x$) and to $|\bar{j}\rangle$ (at $\phi = 2\pi - \phi_x$) change in the same amount, $|\varepsilon_Z|$, but with opposite signs. In general, if the total spin of the Andreev state is not fully aligned with the external magnetic field then the splitting will be a fraction of $|\varepsilon_Z|$ (but still proportional to the magnetic field). We must also keep in mind that the states change their spin structure as ϕ (and ε) varies.

In order to qualitatively understand how phase-shifts may arise due to the Zeeman energy shift, ε_Z, we now particularize to the case of a transparent N-S interfaces in a long junction—a situation in which their Andreev levels can be approximated as linear functions of the phase for $|\varepsilon| < \Delta_0$.[25,47] For $|\varepsilon| < \Delta_0$, we write the levels as

$$\varepsilon_j(\phi,\varepsilon_Z) = \lambda_j(\phi - \pi) - \varepsilon_Z \frac{2}{\hbar}\langle S_{j,y}\rangle\,, \tag{20a}$$

$$\varepsilon_{\bar{j}}(\phi,\varepsilon_Z) = -\lambda_j(\phi - \pi) - \varepsilon_Z \frac{2}{\hbar}\langle S_{\bar{j},y}\rangle\,, \tag{20b}$$

$$= -\lambda_j(\phi - \pi) + \varepsilon_Z \frac{2}{\hbar}\langle S_{j,y}\rangle\,, \tag{20c}$$

where $\lambda_j > 0$ is the slope of the level and $\langle S_{q,y}\rangle$ is the total spin along the y direction of the Andreev state $|q\rangle$ —we later relate these quantities with the parameters of our system. From Eq. (20), we see that the shift in energy, due to the presence of the magnetic field B_y, is equivalent to a shift of the superconducting phase of the Andreev levels at zero field:

$$\varepsilon_j(\phi,\varepsilon_Z) = \varepsilon_j\big(\phi - \phi_j^Z, 0\big)\,, \tag{21a}$$

$$\varepsilon_{\bar{j}}(\phi,\varepsilon_Z) = \varepsilon_{\bar{j}}\big(\phi - \phi_j^Z, 0\big)\,, \tag{21b}$$

$$\phi_j^Z = \frac{2\varepsilon_Z}{\hbar\lambda_j}\langle S_{j,y}\rangle\,. \tag{21c}$$

The energy levels in Eqs. (20) and (21) are single-valued functions in ϕ. However, by translating all solutions to the $[0,2\pi]$ region, we get many Andreev levels for each value of ϕ in that range. The effect of the magnetic field is shown in Fig. 5(a) for an unrestricted phase axis, while Fig. 5(b) shows the same results folded into the $[0,2\pi]$ region. This illustrates

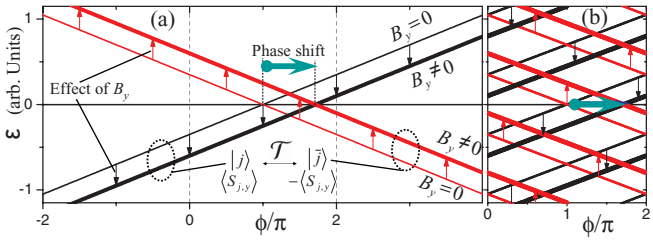

FIG. 5. (Color online) Phase shifts due to external magnetic fields. The N-S interfaces are transparent. (a) Andreev levels in the long junction limit. At zero field, due to the symmetry under $\mathcal{T}$ of the BdG Hamiltonian, for every state $|j\rangle$, at ϕ_x, there is an associated state $|\bar{j}\rangle$, at $2\pi - \phi_x$ ($\equiv -\phi_x$) that (i) has the same energy, (ii) has opposite local spins properties (see text), and (iii) has opposite velocity. A weak in-plane magnetic field B_y—if applied along a direction in which the total spin of the Andreev state is nonzero—generates an increment (decrement) of the energy of the state $|\bar{j}\rangle$ ($|j\rangle$) as shown with vertical arrows. The new pattern of Andreev levels (thick lines) are phase-shifted (horizontal arrow) from the $B = 0$ levels (thin lines). (b) Shows the Andreev levels of (a) restricting ϕ to the $(0,2\pi)$ region.

how the energy levels of a $\mathcal{T}$ pair of Andreev states would rearrange due to the magnetic field in any long junction in the transparent interface limit.

From the above discussion, we see that the $\mathcal{T}$ pairs provide a useful way to group the Andreev levels when discussing how a weak magnetic field can modify them. It is appropriate to make an important remark here. It is known that for a system with zero spin-orbit coupling but nonzero magnetic field the Josephson current fulfills the constrictions of Eq. (17) irrespective of the transparency of the interfaces, the value of the magnetic field and the length of the junction. This follows from a symmetry of the Hamiltonian analog to the one presented in Eq. (15) for time-reversal systems, namely,[27]

$$H_{\mathrm{BdG}}(-\phi) = \mathcal{U}^{-1} H_{\mathrm{BdG}}(\phi)\mathcal{U}\,, \tag{22}$$

where $\mathcal{U} = \mathcal{T}R_\pi$ and R_π is a π rotation of the spin along an axis perpendicular to the one of the magnetic field. The TR operator, $\mathcal{T}$, reverses the magnetic field direction and R_π maps the field back to its original direction. The relation holds even with a position dependent magnetic field, providing the magnetic field is coplanar—the rotation R_π is taken along the normal to such plane. The properties of Eq. (17) for the CPR follow straightforwardly by noticing that the two states in a $\mathcal{U}$ pair [analogous to states in the $\mathcal{T}$ pair of Eq. (16)] have opposite velocities.

The important point is that, for Josephson junctions in which SOC and Zeeman fields coexists, a symmetry operator $\mathcal{U}'$ as the one in Eq. (22) does not exists in general and thus the CPR properties shown in Eq. (17) can be violated: the CPR can have $I(0) \neq 0$, $I(\pi) \neq 0$, and $I_c^+ \neq I_c^-$.[26] It is instructive to discuss, for example, the case of 1D spin-orbit system with a Zeeman field,

$$\mathcal{H}^0 = \frac{1}{2m^*}(p_x - \hbar k_\alpha \sigma_1)^2 - E_\alpha + E_{Z,1}\sigma_1 + E_{Z,3}\sigma_3\,, \tag{23}$$

where we have written the $\{1,2,3\}$ directions in spin space for gaining generality (σ_i are the Pauli matrices) with the SOC along the 1 direction. $E_{Z,1}$ and $E_{Z,3}$ are the parallel and

perpendicular Zeeman energies, respectively. This Hamiltonian can be mapped by a well-known unitary transformation to a system without SOC but with an inhomogeneous magnetic field. The transformation is just the spin-dependent shift in momentum,[50] $U_\alpha = \exp(ik_\alpha x\sigma_1)$. In the transformed Hamiltonian, the parallel magnetic field is unaffected, whereas the perpendicular component rotates along the 1 axis as a function of the position x,

$$U_\alpha^\dagger \mathcal{H}^0 U_\alpha = \frac{p_x^2}{2m^*} - E_\alpha + E_{Z,1}\sigma_1 + E_{Z,3}[\cos(2k_\alpha x)\sigma_3 - \sin(2k_\alpha x)\sigma_2]\,. \quad (24)$$

Notice also that the s-wave superconducting pairing potential transforms trivially under U_α.[51] This simple argument allows us to see that for magnetic fields that are neither parallel nor perpendicular to the SOC axis—i.e., $E_{Z,1} \neq 0$ and $E_{Z,3} \neq 0$—a symmetry as in Eq. (22) cannot be found because the system is intrinsically equivalent to a system without SOC but subject to a non coplanar Zeeman field texture.

For the 2D case with Rashba SOC, it has been shown in Ref. 26 that a symmetry $\mathcal{U}'$ that assures zero Josephson current for $\phi = 0$ can be found only if the Zeeman interaction is perpendicular to the plane of the SOC.[52] For inplane fields, as Eq. (17) no longer holds, current for $\phi = 0$ and $\phi = \pi$ is not forbidden by symmetry and also one may find that $I_c^+ \neq I_c^-$. However, the geometry of the sample plays a crucial role since not any in-plane direction is efficient to modify the Josephson current. For instance, due to the sample configuration (width going to infinity), phase shifts in Ref. 12 are not observed for both directions of in-plane magnetic fields. Similarly, in the finite width stripe geometry we investigate,[22] (with or without a symmetric barrier inside) if the magnetic field is *parallel* to the stripe, the current for $\phi = 0$ becomes zero.

From the above discussion, we have deepened our physical understanding of the presence of a finite Josephson current at zero phase difference. Our TR-symmetric device is able to break the spin degeneracy of the Andreev states in absence of magnetic fields. Due to the sample-specific geometry, a given in-plane direction is privileged in the spin of the Andreev states. More specifically, with a single transverse mode open inside the barrier, the two Andreev states with positive velocity ($|A\rangle$ and $|B\rangle$ states in Figs. 3 and 4) can have the *same* sign of total magnetization *along* the direction in which the SOC device polarizes. From the concepts that led us to Eq. (21), it follows that a nonzero current for zero phase difference is expected if a weak magnetic field B_y is applied as $\phi_A^Z \neq -\phi_B^Z$. On the other hand, current for zero phase difference is not expected for inplane magnetic fields along the x direction because for those states the integrated magnetization along x direction is zero, i.e., $\langle S_{A,x}\rangle = \langle S_{B,x}\rangle = 0$. This is in agreement with our numerical simulations.

3. *Andreev levels and phase shifts in the weak magnetic field limit*

In order to analyze our numerical results quantitatively, we now relate the two essential features of the Andreev states in transparent junctions, namely their phase dependence (slope) and their energies as a function of a magnetic field (in linear response), with the parameters of our system. The energies of Andreev states for a homogeneous and long ($L_N \gg \xi_N \equiv \hbar v_F/\pi\Delta$) one-dimensional S-N-S junction are given by $\varepsilon^{n,\pm} = \hbar v_F/(2L_N)[2\pi(n+1/2) \pm \phi]$, where v_F is the Fermi velocity of the normal material, and L_N is the length of the junction and the plus and minus signs correspond to the two signs of the excitation velocity. This expression can be generalized to include both the effect of external field and corrections of order ξ_N/L_N. Following the procedure of Ref. 25, we obtain

$$\varepsilon_\sigma^{n,\pm} = \sigma\mu_{\rm eff}B_y + \frac{\hbar v_F}{2(L_N + \pi\xi_N)}[2\pi(n+1/2) \pm \phi]\,, \quad (25)$$

here σ is the spin of the Andreev state and $\mu_{\rm eff}$ is the effective magnetic moment

$$\mu_{\rm eff} = \frac{g_N\mu_B}{2}\left(1 + \frac{\frac{g_S}{g_N} - 1}{1 + \frac{L_N}{\pi\xi_N}}\right). \quad (26)$$

We assume that the magnetic field is in the y direction—since it is contained in the plane of the 2DEG no diamagnetic effects are induced. The energies of the Andreev states are then simply shifted by the field. In Eq. (25), n is an integer and ϕ is restricted to the $[0,2\pi]$ region. These energy levels are equivalent to the ones presented in Eq. (20) after folding them into the $[0,2\pi]$ interval, as done in Fig. 5(b).

This analytical result for a 1D system without SOC can be used to qualitatively analyze the effects induced by the presence of a barrier in a normal region when $\alpha \neq 0$. We resort to the WKB approximation and proceed in the following way: for an adiabatic QPC in the absence of external magnetic fields and for an electron (and the reflected hole) in the channel i, we define a "local" wave vector,

$$k_i^{e/h}(x) = F_i^{e/h}(x,\varepsilon,\mu)\,. \quad (27)$$

These functions have to be obtained from the dispersion relations at each position x_a, by assuming that the potential for all x is equal to $V(x_a,y)$. As shown in Sec. II B, due to the SOC the different transverse modes with dispersion relations given by Eq. (7) become mixed and the form of $F_i^{e/h}(x,\varepsilon,\mu)$ become nontrivial—in the absence of SOC, different transverse modes do not mix and the functions are just $F_i^{e/h}(x,\varepsilon,\mu) = \sqrt{\frac{2m^*}{\hbar^2}(\mu \pm \varepsilon) - \widetilde{V}_i(x)}$, with $\widetilde{V}_i(x)$ the effective 1D potential that accounts for the shift of the bottom of the i-channel band.

The orbital phase accumulated by the electron and the reflected hole in the junction is given by

$$\int_0^{L_N} \left[k_i^e(x) - k_i^h(x)\right] dx = \frac{2L_N\delta_i\varepsilon}{\hbar v_F}\,, \quad (28)$$

where we have parametrized the integral by a single dimensionless number δ_i. With this parametrization, we find for the energy of the Andreev states:

$$\varepsilon_{i,\sigma}^{n,\pm} = \frac{\hbar v_F}{2(L_N\delta_i + \pi\xi_N)}[2\pi(n+1/2) \pm \phi]\,. \quad (29)$$

Within this picture, the effect of the barrier only introduces an effective length $L_N\delta_i > L_N$ for each channel—the value of v_F is taken far away from the barrier potential. There is also a small correction to the effective magnetic moment of channel

i that is given by Eq. (26) with L_N replaced by the effective length $L_N\delta_i$.

We found, by inspecting the Andreev levels's slopes of the exact numeric results, that the parameters δ_i are only weakly dependent on the SOC (see below). As the spin is no longer a good quantum number, in the above expression the spin index should be replaced by a new quantum number that characterizes the two branches of each of the $i = 1,2,\ldots,N_{\rm oc}$ transmitted channels. In order to include the effect of an external magnetic field in our simple WKB picture, we profit from the properties of the Andreev states introduced in the previous section. We group the Andreev states in $\mathcal{T}$ partners, $|j\rangle$ and $|\bar{j}\rangle$, given in Eq. (16) [see Fig. 5], where $(j,\bar{j}) = (1,\bar{1}),(2,\bar{2}),\ldots,(2N_{\rm oc},\overline{2N_{\rm oc}})$, and j ($\bar{j}$) labels the states with positive (negative) slope. Therefore, in the linear response regime, a magnetic field B_y leads to the phase shifted energy levels of Eq. (20). In fact, the WKB version of Eq. (20) can be written as

$$\varepsilon_j(\phi) = \eta_j\mu_{\rm eff}B_y + \frac{\hbar v_{\rm F}}{2(L_N\delta_j + \pi\xi_N)}[2\pi(n+1/2)+\phi]\,, \tag{30a}$$

$$\varepsilon_{\bar{j}}(\phi) = -\eta_j\mu_{\rm eff}B_y + \frac{\hbar v_{\rm F}}{2(L_N\delta_j + \pi\xi_N)}[2\pi(n+3/2)-\phi]\,, \tag{30b}$$

where the parameter $|\eta_j| \leqslant 1$ quantifies how different from the spin degenerate case the system behaves. The link between the parameters and the phase-shift ϕ_j^Z defined in Eq. (20) can be written as

$$\lambda_j = \frac{\hbar v_{\rm F}}{2(L_N\delta_j + \pi\xi_N)}\,, \tag{31a}$$

$$|\eta_j\mu_{\rm eff}B_y| = \left|\varepsilon_Z\frac{2}{\hbar}\langle S_{j,y}\rangle\right|, \tag{31b}$$

$$\phi_j^Z = \eta_j\mu_{\rm eff}B_y\frac{2(L_N\delta_j+\pi\xi_N)}{\hbar v_{\rm F}}\,. \tag{31c}$$

The factor $\pi\xi_N$ in the denominator can be neglected in the long junction limit—this is the case of the results presented in Fig. 6 that we discuss below. Introducing the linear dispersions of Andreev levels in Eqs. (12) and (13), the zero magnetic field and zero temperature contribution to the Josephson current of each 1D mode (a set of j and $\bar{j}$ partners) is proportional to the saw-tooth function, $F_{\rm st}(\phi)$,[25,47]

$$I_j(\phi) = \frac{2e\lambda_j}{\hbar}F_{\rm st}(\phi) = \begin{cases} \frac{2e\lambda_j}{\hbar}\frac{\phi}{\pi} & \text{if} \quad 0<\phi\leqslant\pi \\ \frac{2e\lambda_j}{\hbar}\left(\frac{\phi}{\pi}-2\right) & \text{if} \quad \pi<\phi\leqslant 2\pi \end{cases}, \tag{32}$$

which is a 2π-periodic zero-mean function and we have defined it for $\phi\in[0,2\pi]$. For L_N/ξ_N finite, the total current includes the contributions of the Andreev bound states ($|\varepsilon| < \Delta_0$) and of the continuum states ($|\varepsilon| > \Delta_0$).[47] For a perfect 1D channel, the CPR has an abrupt change at $\phi = \pi$, however, in the simulation such jump is slightly smoothed due to the presence of the barrier [see Fig. 3(c)].

We now discuss the effect of the magnetic field on the Josephson current. The gate voltage V_g is set to allow the transmission of a single channel, i.e., $N_{\rm oc} = 1$. Thus there are

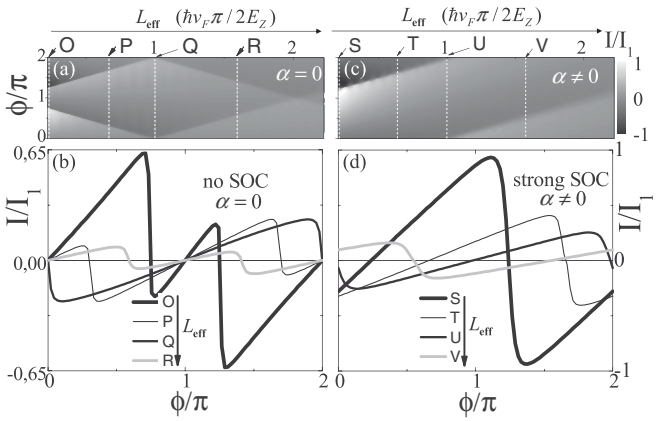

FIG. 6. Josephson current at a fixed finite Zeeman energy, $E_Z = \mu_{\rm eff}B_y$, and a fixed barrier profile—V_g is set to allow transmission of a single transverse mode—as L_N is enlarged. For convenience, we plot it as a function of the effective length, $L_{\rm eff} = \delta_j L_N$ [see Eq. (31c) for $\xi_N \ll L_N$]. (a) and (b) correspond to $\alpha = 0$, whereas (c) and (d) to $\alpha \neq 0$. Qualitatively similar results are obtained if L_N is fixed and E_Z is varied. For $\alpha = 0$, the normal device behaves as a ferromagnetic polarizer; the current at $\phi = 0$ is zero, while changing the length produce 0-π junction transitions. On the other hand, for the case shown for $\alpha \neq 0$, the QPC behaves as an efficient polarizer in the normal state. The magnetic field B_y is applied along the SOC polarization axis. Note that the current at $\phi = 0$ is nonzero and that the phase-shift changes with the length of the junction.

two distinct Andreev levels, $(j,\bar{j}) = (1,\bar{1}),(2,\bar{2})$, with positive and negative slope, respectively. In the simulation, there is a weak in-plane magnetic field (i.e., $E_Z \ll \Delta_0$), and we vary the length of the junction while the barrier dimensions are kept fixed. The quantities $\delta_j L_N$ change and so the phase shifts in Eq. (31a). The current becomes

$$I(\phi) = \frac{2e\lambda_1}{\hbar}F_{\rm st}\left(\phi-\phi_1^Z\right) + \frac{2e\lambda_2}{\hbar}F_{\rm st}\left(\phi-\phi_2^Z\right). \tag{33}$$

We show the CPRs for a system without SOC in Figs. 6(a) and 6(b). Note that there is no current for $\phi = 0$ because the states $j = 1$ and $j = 2$ are the spin-*up* and -*down* states along the y direction, respectively, and so $\phi_2^Z = -\phi_1^Z$ (because $\eta_2 = -\eta_1 = 1$). For $\phi_1^Z = -\phi_2^Z = (2n+1)\pi$, the discontinuity of both saw-tooth functions is at $\phi = 0$. This can be understood as a transition from a 0 to a π junction.

Figures 6(c) and 6(d) show the CPR for a system with polarizing properties due to the presence of strong SOC. The current for $\phi = 0$ is nonzero as both saw-tooth components move in the same direction. This can be understood as follows: as the mode (1,+) dominates the Andreev state $|A\rangle$ [see Figs. 3(e) and 4(a)], we have $\eta_1 = \eta_{\rm A} \approx 1$. On the other hand, since the region of the barrier is small compared to the total length of the junction, the (2,+) mode dominates away from the barrier in the Andreev state $|B\rangle$ [see Figs. 3(f) and 4(b)], and we also have $\eta_2 = \eta_{\rm B} \approx 1$. It then follows that $\phi_2^Z \approx \phi_1^Z$, justifying the numerical results of Fig. 6(c). Using Eqs. (30)–(33), we see that the longer the junction, the bigger the phase shift ($\propto L_N$), while the maximum current gets reduced (because $\lambda_j \propto {L_N}^{-1}$). Similarly, if L_N is fixed, both the phase shift and $I(\phi = 0)$ grow linearly with B_y while the critical current does not change.

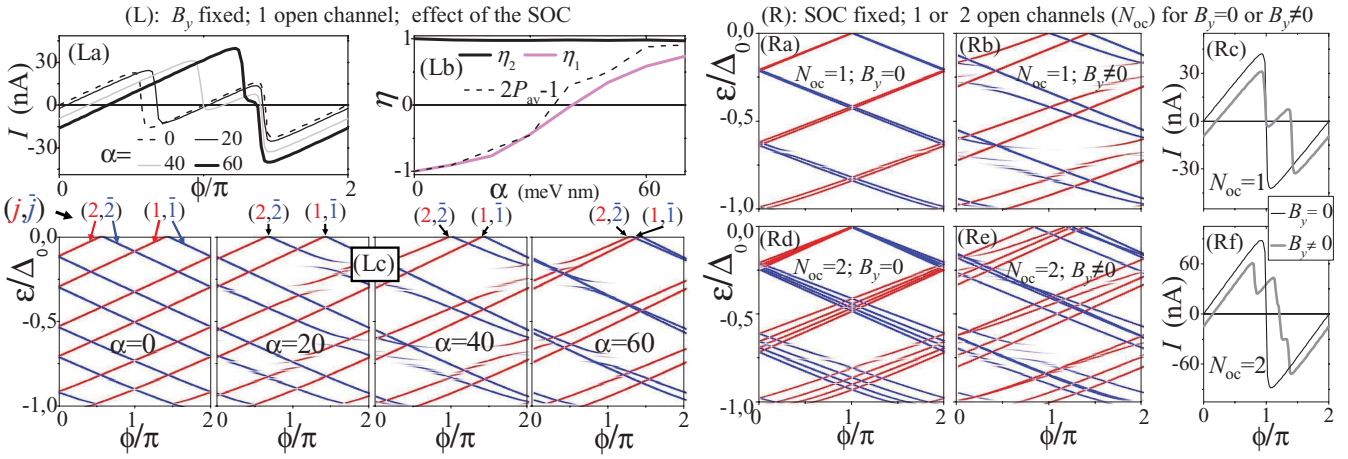

FIG. 7. (Color online) Anomalous current, $I(\phi = 0) \neq 0$, phase-asymmetric CPRs and current-asymmetric CPRs, due to in-plane magnetic field (parallel to the SOC polarization axis). The barrier is the quantum point contact, QPC_1, described by Eq. (A1) taking $(z; W_b; L_b) = (30; 100; 250)$ nm. The junction length is $L_N = 1.2$ μm and the S-N interfaces are transparent. The left (L) panels show CPRs (La) and Andreev levels (Lc) for a fixed magnetic field, $E_Z = g\mu_B B_y = \frac{\Delta_0}{10} = 150$ μeV, and different values of the Rashba strength α. The gate voltage, $V_g = 46.5$ meV, sets the number of open transverse channels, N_{oc}, in 1. The larger α the bigger is the current $I(\phi = 0)$ and the less distorted is the Josephson current from the one at $B_y = 0$: it looks as a phase-shifted version of the CPR at zero field [see (Ra) and (Rc)]. (Lc) Deduced relative magnetic moments, η_1 and η_2, of the two Andreev bound states (see text) as a function of α. We show the simplest estimation for η_2, $(2P_{av} - 1)$, with P_{av} the average polarization induced by the device in the energy range of the superconducting gap. The right (R) panels show how the opening of more than one transverse mode in the QPC can lead to asymmetric CPRs when B_y is nonzero. We fix $\alpha = 40$ meVnm and show the Andreev levels, for $(V_g, N_{oc}) = (46.5$ meV$,1)$ [(39.4 meV,2)] in (Ra) [(Rd)] for $B_y = 0$ and in (Rb) [(Re)] for $B_y \neq 0$: $E_Z = 150$ μeV. In (Rf), the CPR for $B_y \neq 0$ and $N_{oc} = 2$ does show current-asymmetry, i.e., it fulfills Eq. (17). On the other hand, for the case of $N_{oc} = 1$ shown in (Rc), the CPR gets phase shifted and distorted for $B_y \neq 0$ but no strong current-asymmetry is observed.

4. *Phase shift of Andreev levels, dependence with α*

In Fig. 7(L), we show the Andreev levels and the CPRs for several values of α corresponding to the weak, intermediate, and the strong SOC regime. The number of open channels N_{oc} is one and both the junction length and the magnetic field are fixed. As expected, for $\alpha = 0$ [see Fig. 7(Lc)], the arrangement of Andreev levels is symmetric with respect to $\phi = \pi$. We call $(j, \bar{j}) = (1, \bar{1})$ $[(j, \bar{j}) = (2, \bar{2})]$ to the two energy levels that cross $\varepsilon = 0$ at $\phi > \pi$ [at $\phi < \pi$]. Notice that as α is increased the position of the crossing for $(2, \bar{2})$ at $\varepsilon = 0$ shifts in phase to the right, whereas for levels $(1, \bar{1})$, the crossing position remains unchanged. This is interpreted using the WKB picture. We associate levels $(1, \bar{1})$ to states in which electrons and holes do not go through avoided crossings in the transport through the QPC. Therefore, in these states, the spin remains along the y direction: i.e., $\eta_1 \approx +1$, for the Andreev state associated to $|A\rangle$ [see Fig. 4(a)] and its $\mathcal{T}$ partner.

On the other hand, the Andreev states corresponding to levels $(2, \bar{2})$ have their spin not fully aligned to the y direction as electrons and holes are affected by the avoided crossings for nonzero α. In the strong SOC limit, we associate them to the Andreev state $|B\rangle$ [see Fig. 4(b)] and its $\mathcal{T}$ partner. As the probability to follow the avoided crossing increases with α [see, for example, the 2-channels model in Eq. (9)], the wave function in the region away from the barrier is changed from being dominated by the first transverse mode (at $\alpha \approx 0$ holding $\eta_2 = -1$) to being dominated by the second transverse mode with opposite spin along the y direction (at very strong SOC such that $\eta_2 \approx 1$).

For both types of states, we take the slopes of the Andreev levels λ_j and from Eq. (31a) compute the values δ_j. Notice that we have sorted out the $\mathcal{T}$ partners (here $j = 1,2$) by increasing j as λ_j decreases, i.e., from the fastest to the slowest Andreev state. Then we introduce the observed shifts ϕ_j^Z [see Fig. 7(Lc)] in Eq. (30) to compute the parameters η_j. The results are presented in Table I and Fig. 7(Lb) where we plot the values η_j.

In Fig. 7(Lb), we see that, as expected, η_1 is constant as a function of α. We show that η_2 is well approximated by $2P_{av} - 1$, with P_{av} the average polarization of the QPC in the $\varepsilon \in (-\Delta_0, \Delta_0)$ energy window. This quantity is a crude estimate for the spin projection of the Andreev state that suffers the avoided crossing for the case in which the total length of the junction is much larger than the zone of the barrier in which the spin gets mixed. In this limit, one can assume that the spin of the Andreev state is dominated by their spin properties away from the barrier, these being the ones which in the normal device dictate the value of the polarization. More specifically, we assume that $\eta_2 \approx S_2$, with S_2 extracted from the polarization of the normal device. We assume $P_{av} = (1 + S_2)/2$: the factor 2 in the denominator accounts for the total number of transmitted modes within the first conductance

TABLE I. Dependence with α of parameters δ_j and η_j, $j = 1,2$. The JJ has the quantum point contact QPC_1, the CPRs, and Andreev levels are those shown in Fig. 7 (left panels).

α(meVnm)→	0	10	20	30	40	50	60	70
δ_1	1.43	1.43	1.41	1.40	1.42	1.45	1.49	1.52
η_1	1.	0.99	0.99	0.99	0.99	0.98	0.98	0.98
δ_2	1.43	1.43	1.41	1.40	1.39	1.37	1.35	1.34
η_2	−1.	−0.90	−0.77	−0.44	−0.03	0.34	0.59	0.74

plateau and the numerator is the sum of 1 [i.e., full spin *up* due to the electron never leaving the (1,+) mode] with the contribution S_2 given by the specific superposition in modes (1,−) and (2,+) arriving to lead R due to the SOC-induced avoided crossing (see 2-channels model in Sec. II B).

5. *Asymmetric CPRs*

So far, we have shown results for one open channel in the QPC. In the weak-B_y limit, we have shown that a current appears for zero phase difference. This is due to different shifts suffered by each of the two $\mathcal{T}$ partners of Andreev states. As we discuss in Sec. III A2, here the current-phase relation does not need to be symmetric and thus the critical current can depend on the direction of the current flow, i.e., $I_c^+ \neq I_c^-$. We find that the latter effect becomes significant when the barrier is tuned to allow the transmission of a few (more than one) open channels. This is shown in Fig. 7(Rf) for $N_{oc} = 2$. For convenience, we number the $\mathcal{T}$ couples $j = 1,2,\ldots,2N_{oc}$ from faster to slower Andreev states (decreasing slope of their dependance on ϕ). In the case of Figs. 7(Rd) and 7(Re), we show how four of those couples ($N_{oc} = 2$) rearrange due to a finite magnetic-field applied along the direction of polarization. In Table II, we present the parameters δ_j and η_j obtained from the simulations.

As expected the fastest $\mathcal{T}$ pair ($j = 1$) has $\eta_1 \approx 1$ due to the fact that they are associated with Andreev states in the outermost branches of (1,+) and (1,−), i.e., those unaffected by avoided crossings. The remaining three $\mathcal{T}$ pairs are affected by the avoided crossings in the transport through the barrier. Each of them also sees a different effective length ($\delta_j L_N$) in the passage through the barrier. This combination of different slopes and different spin properties (η_j) translates, given a finite magnetic field along the y direction, into an asymmetric CPR. The asymmetry is difficult to detect in the same device for the $N_{oc} = 1$ case (at a higher gate voltage). In Figs. 7(Ra) and 7(Rb), we show that the rearrangement of Andreev levels for $N_{oc} = 1$ is symmetrical (with respect to a new phase value different from π) except for the small difference in slopes between the two $\mathcal{T}$ pairs; the latter difference does not produce a significant asymmetry in the total CPR shown in Fig. 7(Rc).

The significant difference of the two critical currents, $|I_c^+ - I_c^-|/(I_c^+ + I_c^-)$, also gets reduced in the opposite limit, when $N_{oc} \gg 1$. In this case, the full current is the sum of the contributions of the $2N_{oc}$ $\mathcal{T}$ pairs and balanced spin properties are dominant since a smaller fraction of the transmitted channels undergo an avoided crossing transition. This can be understood, for example, by taking the height of the barrier half of what is considered in Fig. 1. Then, the electrons in channels (1,−) traveling from left to right would not be affected by the avoided crossings with mode (2,+) and thus both modes (1,σ) would be transmitted. Assuming that the third transverse mode can now transmit, only the SOC mixing between (2,σ) and (3,$\bar{\sigma}$) modes contributes to spin filtering effect. This is the reason why the polarization, and thus the anomalous Josephson effects we study here, is smaller when many channels are allowed to transmit through the barrier.

TABLE II. Values of δ_j and η_j for two open channels in the QPCs for different junction lengths when $\alpha = 40$ meVnm.

V_g (meV)	L_N (nm)	δ_1	η_1	δ_2	η_2	δ_3	η_3	δ_4	η_4
QPC_1	600	1.39	0.95	1.49	0.50	1.63	−0.31	1.82	0.18
39.4	900	1.27	0.97	1.35	0.55	1.44	−0.41	1.58	0.27
	1200	1.21	0.99	1.27	0.58	1.33	−0.45	1.47	0.36
QPC_2	600	1.53	0.97	1.60	−0.84	1.70	0.87	1.90	0.72
46.3	900	1.40	0.97	1.45	−0.85	1.52	0.89	1.66	0.77
	1200	1.31	0.99	1.36	−0.86	1.41	0.90	1.52	0.79

B. Anomalous Josephson effects enhanced by barriers with SOC: Nonideal interfaces

In the previous section, the analysis was deliberately made to elucidate the effects introduced by the barrier. Therefore we have idealized the S-N junctions in order to minimize normal reflections at the S-N interface. In those simulations, the matching between 2DEG and superconductors was very good despite the fact that the latter have $\alpha = 0$ and a smaller g factor. Here, we change the superconductor system, as described in Sec. II A,[22] with the goal of incorporating the mismatch of Fermi velocities between the 2DEG and the S contacts to simulate more realistic experimental devices.[21] In the following, we show that anomalous effects in the CPR due to the polarizing effects are present both for realistic junctions based on quantum point contacts and for wide barriers.

1. *Quantum point contacts*

The drastic effect of more realistic 2DEG-contact interfaces was discussed in Sec. II B3 for the transport properties of QPCs when the leads were taken to be metallic, i.e., $\Delta_0 = 0$. As shown in Fig. 2—for a ratio between Fermi velocities, $v_F^{2DEG}/v_F^{Nb} \approx 2.25$ —the conductance through the QPC shows a resonant-like behavior as a function of gate-voltage. In particular, we have shown that, due to quantum interference effects, the polarization peaks can be larger than the polarization developed for the case where the 2DEG-contacts interfaces do not generate backscattering.

Figure 8 show results derived from the current-phase relation in a Josephson junction containing a QPC and realistic 2DEG-S interfaces. Due to the magnetic field B_y, the CPR for the system has interesting properties that can be tuned by changing the gate voltage, which controls the barrier height. For convenience, we define the average critical current [see Fig. 8(a)]

$$\bar{I}_c \equiv \tfrac{1}{2}(I_c^+ + I_c^-)\,, \tag{34}$$

the anomalous current [or zero phase difference current, see Fig. 8 (b)]

$$I_a \equiv I(\phi = 0)\,, \tag{35}$$

and the asymmetry of the CPR [see the dependence with E_Z in Fig. 8(c)]

$$\text{Asymmetry} \equiv \frac{I_c^+}{I_c^-}\,. \tag{36}$$

The underlying resonant tunneling physics produce an abrupt dependence with the gate voltage of the quantities of interest. This is different from the idealized S-N junctions case of Sec. III A for which the results do not change with V_g providing

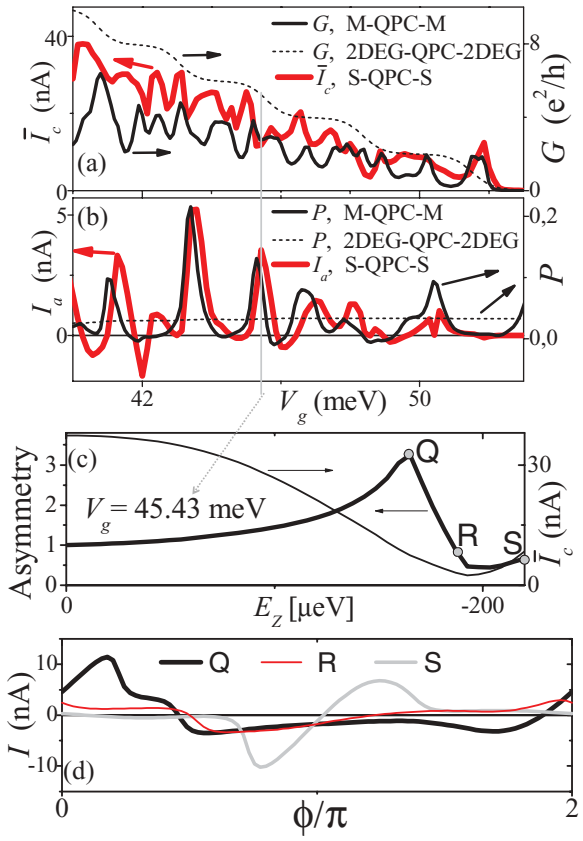

FIG. 8. (Color online) Results for a Josephson junction, S-QPC-S, based in QPC_2 with realistic 2DEG-S junctions: an In-based 2DEG and Nb superconductors are simulated [parameters given in Fig. 2(b)]. We take $\alpha = 5$ meVnm, $L_N = 1.2\ \mu$m; in (a) and (b) for the JJ results the Zeeman energy in the 2DEG is $E_Z = -150\ \mu$eV. We plot the dependence with the gate voltage V_g of: (a) the average critical current $\bar{I}_c$ and (b) the anomalous Josephson current I_a. In (a) [(b)], we include the conductance G [the polarization P] as a function of V_g for the same device between normal contacts (dashed line, 2DEG-QPC-2DEG junction), such that the leads do not generate backscattering and the leads are metallic (solid black line, M-QPC-M junction), we take the parameters of Nb with $\Delta_0 = 0$. We observe correlation between $\bar{I}_c(I_a)$ for the S-QPC-S and $G(P)$ for the M-QPC-M. (c) We fix V_g at a peak for I_a and present, as a function of E_Z, $\bar{I}_c$ and the critical current asymmetry I_c^+/I_c^-. For such value of V_g, the departure from the $I_c^+ = I_c^-$ situation is strong and controllable via magnetic field (and gate voltage as shown in Ref. 22). (d) We plot the full current-phase relations for some situations labeled in (c).

the number of open channels in the QPC remains the same. The dependence with V_g shows resonant peaks in both $\bar{I}_c$ and I_a. Figure 8(d) presents some examples of CPRs that show a striking asymmetry. In these cases, the fact that the CPRs fulfill the zero area condition of Eq. (14) is not obvious.

Indeed, because of the strong normal reflection at the interfaces, the system can be interpreted as a S-quantum dot-S Josephson junction and thus the resonant-like shapes in the critical current are expected.[48] This is the so-called resonant tunneling supercurrent transistor regime for samples in which the charging energy of the "dot" is small and thus Coulomb blockade is not observed.[53,54] In the absence of a magnetic field, the states arising in the quantum dot appear as time reversal pairs. As for the case of Sec. III A, for JJs based on normal quantum dots with spin-orbit coupling, no asymmetric CPRs or current for zero phase difference are expected at zero field.[17]

A correlation between the normal transport and the superconducting transport is observed in the shapes of $\bar{I}_c$ and G in Fig. 8(a). This is understood generically, for Josephson transistor devices, because the critical current is dominated by the contribution of the highest quasiparticle level (i.e., closest to $\varepsilon = 0$).[53] Then the critical current is maximized at the same values of V_g that maximize G in the M-QPC-M device: constructive interference favors transmission of quasiparticles and Andreev bound states acquires strong dependence with the phase ϕ for $\varepsilon \approx 0$. Moreover, in Fig. 8(b), we find a strong correlation between P in the normal device and the anomalous current I_a in the associated Josephson junction.

Here, the fact that the transport is conditioned by normal backscattering at the interfaces and interference effects does not invalidate the symmetry arguments discussed in Sec. III A for the existence of Andreev states $\mathcal{T}$ partners at zero magnetic field. Indeed, the Andreev states at a resonant condition are $\mathcal{T}$ partners and it is natural to expect that their spins [see Eq. (19)] are correlated with the polarization found in the corresponding normal junction. At the resonant value of V_g, their associated Andreev levels cross each other with opposite slopes at $(\varepsilon,\phi) = (0,\pi)$.[54] In a zero SOC system, Andreev states are spin degenerate and thus there are two $\mathcal{T}-$pairs resonating at the same V_g. Here, on the other hand, as pointed out in Sec. II B, the two scattering states contributing to a given transverse mode have different velocities. In the Fabry-Perot geometry, this leads to resonances at different values of V_g. In summary, the multichannel physics, the symmetric sample geometry, and the SOC make a particular spin projection, *up* along the y direction in this case, to be favored in the normal transport from left to right ($P_{L\to R} > 0$). The opposite projection is favored in the right to left normal transport. The Fabry-Perot effects enhances the polarizing effect for specific values of V_g. In the associated Josephson junction, when a weak B_y breaks the spin degeneracy, this leads to a nontrivial rearrangements of the Andreev levels resulting in the nonzero I_a and/or asymmetric CPRs, $I_c^+ \neq I_c^-$.

It is worth mentioning that the biggest asymmetry in the CPR occurs due to the magnetic field for the cases which at zero field present a few off-resonance $\mathcal{T}$ pairs (i.e., pairs whose energies are below the Fermi energy for any value of the phase difference) and a single resonant $\mathcal{T}$ pair (its energy reaches $\varepsilon = 0$ for $\phi = \pi$). In this situation, the dispersion of the resonant Andreev state is close to the one corresponding to the ballistic case, while the off-resonant ones are more sinusoidal-like, typical of a low transmission channel (results not shown). Therefore the shifts induced by the B field are very different in each case, leading to the observed asymmetry when the corresponding contributions to the CPR are added up. This becomes strongly dependent on V_g allowing, at a fixed B, to use slight changes in the gate voltage as a control parameter.[55] The $I_c^+ \neq I_c^-$ condition is generically observed as long as few open channels are open in the QPC and the modes affected by SOC mixing contribute a significative fraction of the total current. We observe that the asymmetry grows with the magnetic field as shown in Fig. 8(c) up to a value in which it jumps from

$I_c^+ > I_c^-$ to $I_c^+ < I_c^-$. This dependence is also observed at fixed B_y as a function of the junction length—in such a case, one has to change V_g with L_N in order to follow the resonant condition. The qualitative interchangeability of L_N and B_y, as in S-F-S junctions, follows because both quantities produce an enhancement of the underlying phase-shifts of Andreev levels (see Sec. III A 3).

2. *Wide barriers*

In Sec. II B, we have presented the polarizing properties of QPCs.[28] The WKB picture, in Fig. 1, shows therefore transverse modes well separated in energy by virtue of the transversal quantization induced by the lateral constriction of the QPC. The polarizing properties, however, are also expected for very wide barriers. The physical mechanism is conceptually the same, i.e., a smaller transverse modes quantization energy does not avoid the SOC-induced mode mixing leading to polarization in the transport through an adiabatic barrier. This nontrivial spin transport shares the same time-reversal properties as in the discussed QPC. Nonzero polarization has been derived by Silvestrov and Mishchenko in Ref. 29 even for the case of a very wide system with transversal periodic conditions. As the barrier (B) becomes smaller the polarization decreases in agreement with the observations in QPCs. Here we present results for the polarization in a wide barrier and show that these devices also lead to the same CPR phenomena in Josephson junctions.

Figure 9 shows results for the wide barrier potential $V_{\text{wide}}(x,y)$ given in Appendix. The barrier has no dependence with y and thus lateral confinement is determined by the stripe width W_y chosen in the simulation. We take $W_y = 630$ nm, which means 51 open channels in the stripe ($V_g = 0$) for our choice of the Fermi energy. We denote with $Z = 0$ to the case of a 2DEG-B-2DEG junction, i.e., the leads are essentially the same material as the central region except from the reduced g factor and the zero spin-orbit coupling—recall that Z is the amplitude of the barriers at the S-N junctions in the BTK approach.[39] Then we study the case in which the leads are metallic, i.e., a M-B-M junction. In the latter case, we use the parameter A presented in Eq. (6), to reduce the transparency of the junction away from the ideal condition ($A = 1$).

In Fig. 9(a), we shown the normal transport properties of the barrier, the conductance G and the polarization P, that we use to characterize it. In the $Z = 0$ case, despite the fact that the conductance plateaux become undefined, the polarization is nonzero. In the case of metallic leads with high transparency, $A = 1$, the G and P acquire some structure but without showing marked resonances as in the QPC case. This can be understood from the fact that many channels with similar velocity are available and thus neighboring resonances overlap. The total contribution is similar to the $Z = 0$ case except for a reduction of the conductance. When we take $A = 0.3$, the transparency of the junction is decreased and both the conductance and polarization are affected. In particular, the polarization shows peaks as a function of V_g.

We transform all these cases into Josephson junctions by taking $\Delta_0 = 1.5$ meV. The current-phase relations in the presence of a finite magnetic field along the y direction is shown in Fig. 9(b). We can easily find, by tuning V_g, situations with $I_a \neq 0$ and asymmetric CPRs. As it is the case for QPCs, the asymmetry of the CPRs becomes larger for the realistic junctions having normal scattering at S-N interfaces. The phenomena is smaller the more modes are allowed to transmit in the device as it is also the case for the polarization of the associated normal device.

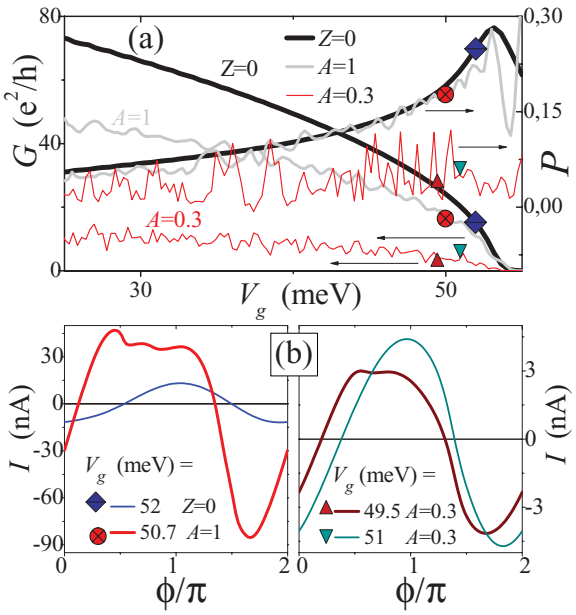

FIG. 9. (Color online) Results for a junction with potential $V_{\text{wide}}(x,y)$ with $L_b = 360$ nm, i.e., a plain barrier (B) without a lateral constriction. We take $\alpha = 20$ meVnm and the 2DEG and superconductor parameters given in Figs. 2 and 8. (a) Spin polarizing properties of the barrier when the leads are normal, we show the dependence on gate voltage V_g for the conductance G and the polarization P. Case $Z = 0$ is for a 2DEG-B-2DEG junction, i.e., the interfaces are ideal as the leads are the same In-based 2DEG. The other two cases are for the M-B-M junction, the leads are metallic Nb and a there is mismatch of Fermi velocities and effective masses; moreover, away from $A = 1$, see Eq. (6), the transparency of the junction is decreased. (b) The normal systems of (a) are turned into Josephson junctions due to a superconducting pairing $\Delta_0 = 1.5$ meV in the contacts and we also include a Zeeman field along the y axis with energy $E_Z = -150\ \mu$eV. Current-phase relations showing both current for $\phi = 0$ and/or CPR asymmetry $I_c^+ \neq I_c^-$, as those appearing in QPCs, can also be obtained for wide barriers.

IV. CONCLUSIONS

We have described how the spin-polarizing properties of barriers with spin-orbit interaction affect the spin of the Andreev states. First, we revisited the normal device polarization mechanism highlighting the multichannel nature of the transport while stressing that the polarization of the transmitted electrons is due to the mode mixing induced by the SOC term proportional to the transversal linear momentum. As the device is time-reversal-symmetric strong restrictions are imposed on the spin-resolved transmissions in opposite directions. At zero magnetic field, the properties derived from these restrictions do not conspire against the formation of Andreev bound states, this is opposite to the case of ferromagnetic polarizers.

At zero magnetic field, a symmetry of the BdG equation,[26] including the SOC, links Andreev states corresponding to

phase differences between superconductors $+\phi_x$ and $-\phi_x$, respectively, that have opposite spin and velocity. The symmetry argument is valid for the junction irrespective of the transparency of the S-N interfaces. Each of these states, that would appear spin-degenerate in the absence of SOC, are nondegenerate in its presence. More remarkable, the polarizing barrier makes the two Andreev states traveling in the same direction for $+\phi_x$ (with slightly different energy due to SOC) to share similar spin properties. Because of the mentioned symmetry there are two Andreev states for $-\phi_x$ that travel in the opposite direction having spin opposite to those for $+\phi_x$, so the system presents a spin *chirality*. In our system, we have shown that the introduction of a weak magnetic field along the direction in which the Andreev states are spin chiral is enough to trigger anomalous Josephson effects such as current at zero phase difference I_a and $I_c^+ \neq I_c^-$. The chirality condition here is built into the device properties by the presence of the barrier and thus it can be switched on and off with gate voltage. The condition is similar to the one required for nonzero anomalous current in the spin-orbit coupled quantum dot Josephson junction of Ref. 18. As this spin chirality is intrinsic to other helical systems, we expect that a similar effect could occur in those cases too. That is, a Zeeman-induced I_a would also appear if the B field is aligned with the helical direction in Josephson junction based on s-wave superconductors.[14,26]

In order to see how the spin-polarizing properties of the barrier determine the Andreev states and affect the Josephson effect, we have idealized the S-N interfaces to minimize normal scattering. The numerical results agree with a simple picture for the transport through the barrier, based on the analysis of the contribution of two almost degenerated Andreev states with the same velocity and spin for a given phase difference. In this limit, a direct translation of Zeeman energy shifts into phase-shifts of Andreev levels can be made because of the linearity of the phase dispersion of the Andreev levels in the long junction regime. This, combined with the spin chirality of Andreev states, leads to $I_a \neq 0$. We have studied the dependence of the phase-shifts with junction length, magnetic field and SOC strength. We also showed that asymmetric CPRs are possible when the barrier allows more than one open channel.

We also presented results for QPC based junctions with realistic S-N interfaces. The asymmetry of the CPRs becomes more marked than in the transparent junction case. This is related to the Fabry-Perot like transport that produces peaks in the conductance and polarization of the associated normal device (taking $\Delta_0 = 0$ in the leads).

The phenomena described here are to be expected in barriers as long as the device behaves as a polarizer—due to the mode mixing induced by the SOC. Then, few open channels are preferred. We have shown that anomalous effects are also observable in wide barriers even in cases in which the transparency of the S-N interfaces are not high. Therefore, for smooth barriers with few open channels in quantum wires, the mentioned effects should be observed as long as the spin-orbit coupling is two dimensional, i.e., it must have terms both proportional to the longitudinal momentum and to the transversal momentum. As for quantum wires constriction-type barriers are difficult to implement, the latter is an important result: apart from the practical possibilities arising from the supercurrent rectifier and the phase shifted CPR, the experimental observation of the effects would provide a signature of the presence of a SOC term proportional to the transverse momentum. We believe this is valuable information as SOC is one of the fundamental ingredients required in quantum wires for accessing the topological superconducting phase, and knowledge of all existing SOC terms is desirable.

ACKNOWLEDGMENTS

We acknowledge useful discussions with K. Flensberg, S. De Franceschi, L. Kouwenhoven, and A. Zazunov. AAR acknowledges support from the Australian Research Council Centre of Excellence scheme CE110001013 and from ARO/IARPA project W911NF-10-1-0330. AAR is grateful for the hospitality of the Institut Néel. GU and CAB acknowledge financial support from PICTs 2008-2236 and Bicentenario 2010-1060 from ANPCyT and PIP 11220080101821 from CONICET, Argentina. D.F. and M. A. acknowledge support from ECOS-SECyT collaboration program A06E03 and PICS 05755 from CNRS.

APPENDIX

1. Potential Barrier

To describe the quantum point contact we use the realistic potential given in Ref. 56 for a split-gate defined QPC,

$$
\begin{aligned}
V_{\mathrm{QPC}}(x,y) &= \frac{V_g \Upsilon(x-x_c, y-y_c)}{\Upsilon(0,0)}, \\
\Upsilon(x,y) &= f\left(\frac{2x-L_b}{2z}, \frac{2y+W_b}{2z}\right) - f\left(\frac{2x+L_b}{2z}, \frac{2y+W_b}{2z}\right) + f\left(\frac{2x-L_b}{2z}, \frac{W_b-2y}{2z}\right) - f\left(\frac{2x+L_b}{2z}, \frac{W_b-2y}{2z}\right), \\
f(u,v) &= \frac{\pi}{2} - \arctan u - \arctan v + \arctan \frac{uv}{\sqrt{1+u^2+v^2}},
\end{aligned}
\tag{A1}
$$

where z is the distance between the 2DEG and the plane of the gates, L_b is the length of the gate, W_b is the width of the constriction, and V_g is the value of the potential at the saddle point located at (x_c, y_c).

In the case of barriers without the lateral constriction, we use a modified version of the potential given in Ref. 57,

$$
V_{\mathrm{wide}}(x,y) = \begin{cases} \frac{V_g}{2}\left[1+\cos\left(\frac{\pi(x-x_c)}{L_b}\right)\right] & \text{for } -L_b < x - x_c < L_b \\ 0 & \text{otherwise} \end{cases},
\tag{A2}
$$

where $2L_b$ is the barrier length and at the center of the barrier x_c, the barrier achieves its maximum value V_g.

2. Tight-binding model

Following standard finite-difference procedures for a square lattice with spacing a_0, we write the total Hamiltonian as

$$\hat{H} = \hat{H}_Z + \hat{H}_N + \hat{H}_L + \hat{H}_R + \hat{H}_{N,L} + \hat{H}_{N,R}\,. \tag{A3}$$

For convenience, we have used the same notation as the continuous Hamiltonians given in Sec. II A and we have introduced the Hamiltonians $\hat{H}_{N,\gamma}$ connecting the normal region and the lead $\gamma = \{L,R\}$. The Hamiltonian (2) for the normal region becomes

$$\begin{aligned}\hat{H}_N = \sum_{\boldsymbol{r}\in \mathrm{N},\sigma} &(4t_N + V(\boldsymbol{r}) - \mu)\hat{c}^\dagger_{\boldsymbol{r},\sigma}\hat{c}_{\boldsymbol{r},\sigma} + \Bigg[\sum_{\boldsymbol{r}\in \mathrm{N},\sigma} t_N \hat{c}^\dagger_{\boldsymbol{r},\sigma}\hat{c}_{\boldsymbol{r}+a_0\hat{\mathbf{x}},\sigma} \\ &+ \sum_{\boldsymbol{r}\in \mathrm{N},\sigma} t_N \hat{c}^\dagger_{\boldsymbol{r},\sigma}\hat{c}_{\boldsymbol{r}+a_0\hat{\mathbf{y}},\sigma} - \sum_{\boldsymbol{r}\in \mathrm{N},\sigma} \lambda_{x,\sigma\bar{\sigma}}\hat{c}^\dagger_{\boldsymbol{r},\sigma}\hat{c}_{\boldsymbol{r}+a_0\hat{\mathbf{x}},\bar{\sigma}} \\ &- \sum_{\boldsymbol{r}\in \mathrm{N},\sigma} \lambda_{y,\sigma\bar{\sigma}}\hat{c}^\dagger_{\boldsymbol{r},\sigma}\hat{c}_{\boldsymbol{r}+a_0\hat{\mathbf{y}},\bar{\sigma}} + \mathrm{H.c.}\Bigg],\end{aligned} \tag{A4}$$

where $\hat{c}_{\boldsymbol{r},\sigma}$ ($\hat{c}^\dagger_{\boldsymbol{r},\sigma}$) refers to the annihilation (creation) operator for an electron in the 2DEG at position $\boldsymbol{r}$ with spin $\sigma_z = \sigma = \{\uparrow,\downarrow\}$. The hopping is $t_N = \hbar^2/2m^*a_0^2$. The summations are taken over all lattice sites in the normal region, N; terms with operators $\hat{c}_{\boldsymbol{r},\sigma}$ and $\hat{c}^\dagger_{\boldsymbol{r},\sigma}$ with $\boldsymbol{r}$ outside such region are taken to be zero. The Rashba spin-orbit coupling parameters are related to the Rashba strength in the continuous model as

$$\begin{aligned}\lambda_{x,\uparrow\downarrow} &= \frac{\alpha}{2a_0}, \quad \lambda_{x,\downarrow\uparrow} = -\frac{\alpha}{2a_0}, \\ \lambda_{y,\uparrow\downarrow} &= -\mathrm{i}\frac{\alpha}{2a_0}, \quad \lambda_{y,\downarrow\uparrow} = -\mathrm{i}\frac{\alpha}{2a_0}.\end{aligned} \tag{A5}$$

Notice that time-reversal symmetry is intrinsic to the SOC coupling as we have $\lambda_{j,\sigma\bar{\sigma}} = -(\lambda_{j,\bar{\sigma}\sigma})^*$ with $j = \{x,y\}$.

The lattice version of the Hamiltonian of the leads (1) is

$$\begin{aligned}\hat{H}_\gamma = \sum_{\boldsymbol{r}\in R_\gamma,\sigma} &(4t_S + E_S - \mu)\hat{d}^\dagger_{\boldsymbol{r},\sigma}\hat{d}_{\boldsymbol{r},\sigma} - \Bigg[\sum_{\boldsymbol{r}\in R_\gamma,\sigma} t_S \hat{d}^\dagger_{\boldsymbol{r},\sigma}\hat{d}_{\boldsymbol{r}+a_0\hat{\mathbf{x}},\sigma} \\ &+ \sum_{\boldsymbol{r}\in R_\gamma,\sigma} t_S \hat{d}^\dagger_{\boldsymbol{r},\sigma}\hat{d}_{\boldsymbol{r}+a_0\hat{\mathbf{y}},\sigma} + \Delta_0 \sum_{\boldsymbol{r}\in R_\gamma,\sigma} \hat{d}^\dagger_{\boldsymbol{r},\uparrow}\hat{d}^\dagger_{\boldsymbol{r},\downarrow} + \mathrm{H.c.}\Bigg],\end{aligned} \tag{A6}$$

where $\gamma = \{R,L\}$ for the right and left leads, respectively, the summations are taken over sites belonging to the regions of those leads R_γ and $\hat{d}_{\boldsymbol{r},\sigma}$ ($\hat{d}^\dagger_{\boldsymbol{r},\sigma}$) refers to the annihilation (creation) operator for an electron in the lead γ at position $\boldsymbol{r}$ with spin $\sigma_z = \sigma = \{\uparrow,\downarrow\}$. We use the parameters t_S and E_S for simulating the different types of leads.

When the goal is to minimize the scattering at the leads we use $E_S = 0$ and $t_S = t_N$ [and $A = 1$, see Eq. (6)]. On the other hand, for simulating realistic superconducting leads (or metallic ones if $\Delta_0 = 0$), we change both E_S and t_S assuring that the lead has many open channels—with the appropriated velocity (dispersion)—in a large energy window around the Fermi energy. The size of the latter is not important in the metallic phase, as the low-temperature transport is dominated by the quantum transmission at the Fermi energy. In the superconducting case, it is enough to consider an energy window of a few Δ_0, as the Josephson current in S-N-S junctions is mediated by Andreev reflection, which decays exponentially as a function of energy for $|\varepsilon| > \Delta_0$.[39] The contribution to the CPR of states at energies outside this window is negligible.

In writing the Hamiltonians $\hat{H}_\gamma$, we have chosen a gauge where the superconducting phases $(\phi_l,\phi_r) = (0,-\phi)$ and ϕ is accumulated only in the tunneling Hamiltonian between the central 2DEG and the right superconducting lead.[35] We group the lattice sites according to the coordinate x. The set X_R (X_L), having the sites at $x = x_R$ ($x = x_L$), is the last (first) vertical layer in the normal region. The intermediate Hamiltonians are

$$\begin{aligned}\hat{H}_{N,\gamma} = \Bigg[&-\sum_{\boldsymbol{r}\in X_\gamma,\sigma} t_b \mathrm{e}^{\mathrm{i}\vartheta_\gamma}\hat{c}^\dagger_{\boldsymbol{r},\sigma}\hat{d}_{\boldsymbol{r}+s_\gamma a_0\hat{\mathbf{x}},\sigma} \\ &+ \sum_{\boldsymbol{r}\in X_\gamma,\sigma} \frac{\lambda^\gamma_{\sigma\bar{\sigma}}}{2}\mathrm{e}^{\mathrm{i}\vartheta_\gamma}\hat{c}^\dagger_{\boldsymbol{r},\sigma}\hat{d}_{\boldsymbol{r}+s_\gamma a_0\hat{\mathbf{x}},\bar{\sigma}} + \mathrm{H.c.}\Bigg],\end{aligned} \tag{A7}$$

with parameters $(s_L,\lambda^L_{\uparrow\downarrow},\lambda^L_{\downarrow\uparrow},\vartheta_L) = (-1,\lambda^*_{x,\downarrow\uparrow},\lambda^*_{x,\uparrow\downarrow},0)$ and $(s_R,\lambda^r_{\uparrow\downarrow},\lambda^r_{\downarrow\uparrow},\vartheta_r) = (1,\lambda_{x,\uparrow\downarrow},\lambda_{x,\downarrow\uparrow},-\phi/2)$. Notice that the variation of the Rashba strength—as α is taken to be zero in the leads and nonzero in the central region—introduces a SOC contribution to the tunneling Hamiltonian at the interfaces. This follows as a result of the correct discretization of the SOC term $\frac{\alpha(x)}{\hbar}p_x\sigma_y$—when $\frac{d\alpha(x)}{dx} \neq 0$, i.e., at $x = x_L$ and $x = x_R$, this term needs to be symmetrized to be Hermitian.

Finally, the Zeeman term in the normal region is just

$$\begin{aligned}\hat{H}_Z = \frac{g\mu_B}{2}\Bigg\{&\sum_{\boldsymbol{r},\sigma}(\delta_{\uparrow,\sigma} - \delta_{\downarrow,\sigma})B_z\hat{c}^\dagger_{\boldsymbol{r},\sigma}\hat{c}_{\boldsymbol{r},\sigma} \\ &+ \Bigg[\sum_{\boldsymbol{r}}(B_x - \mathrm{i}B_y)\hat{c}^\dagger_{\boldsymbol{r},\uparrow}\hat{c}_{\boldsymbol{r},\downarrow} + \mathrm{H.c.}\Bigg]\Bigg\}.\end{aligned} \tag{A8}$$

The Zeeman interaction at the leads $\gamma = \{L,R\}$ has the same form but in terms of the operators $\hat{d}_{\boldsymbol{r},\sigma}$ and $\hat{d}^\dagger_{\boldsymbol{r},\sigma}$ with summations taken for $\boldsymbol{r} \in R_\gamma$ and g_N replaced by g_S.

a. Conductance and polarization

For the normal case ($\Delta_0 = 0$), we compute the transport properties in the linear response regime. The conductance follows from

$$G = \frac{e^2}{h}\mathrm{Tr}[\boldsymbol{\Gamma}^L\boldsymbol{G}^r(E_\mathrm{F})\boldsymbol{\Gamma}^R\boldsymbol{G}^a(E_\mathrm{F})]\,, \tag{A9}$$

where $\boldsymbol{G}^{r(a)}(\varepsilon)$ is the retarded (advanced) matrix propagator, with elements $\boldsymbol{G}^r_{\boldsymbol{r}\sigma,\boldsymbol{r}'\sigma'}(\varepsilon)$ given by the propagator from site $\boldsymbol{r}'$ and spin σ' to site $\boldsymbol{r}$ and spin σ, $\boldsymbol{\Gamma}^\gamma_{\boldsymbol{r}\sigma,\boldsymbol{r}'\sigma'} = \mathrm{i}(\boldsymbol{\Sigma}^r_\gamma - \boldsymbol{\Sigma}^a_\gamma)_{\boldsymbol{r}\sigma,\boldsymbol{r}'\sigma'}$ where $\boldsymbol{\Sigma}^{r(a)}_\gamma$ is the retarded (advanced) self-energy due to the γ lead and E_F is the Fermi energy.

The polarization is

$$P = \frac{1}{G}\sum_\sigma (G_{\uparrow\sigma} - G_{\downarrow\sigma})\,, \tag{A10}$$

with $G_{\sigma'\sigma}$ the spin-resolved conductances, i.e., the contributions due to the electrons that are injected from lead L with spin σ and collected at lead R with spin σ'. As the current flow is in the x direction, the relevant polarization occurs for the y axis—recall that the Rashba SOC is proportional to $p_x\sigma_y$. Thus Eq. (A10) refers to the spin-resolved conductances with $\sigma = \{\uparrow,\downarrow\}$ along the y-axis. The polarizations along the x and z spin axis are zero.

b. Josephson current

The Josephson current (12), being proportional to $\langle\frac{\partial\hat{H}}{\partial\phi}\rangle$, follows from $\hat{H}_{N,r}$ as it is the only term in $\hat{H}$ that depends on ϕ,

$$I = \frac{2e}{\hbar}\mathrm{i}\Bigg(\sum_{\sigma,\boldsymbol{r}\epsilon X_R}\left[-\frac{t_b}{2}e^{-\mathrm{i}\frac{\phi}{2}}\langle\hat{c}^\dagger_{\boldsymbol{r},\sigma}\hat{d}_{\boldsymbol{r}+a_0\hat{x},\sigma}\rangle + \frac{t_b}{2}e^{\mathrm{i}\frac{\phi}{2}}\langle\hat{d}^\dagger_{\boldsymbol{r}+a_0\hat{x},\sigma}\hat{c}_{\boldsymbol{r},\sigma}\rangle\right] + \sum_{\boldsymbol{r}\epsilon X_R}\left[\frac{\lambda_{x,\uparrow\downarrow}}{4}e^{-\mathrm{i}\frac{\phi}{2}}\langle\hat{c}^\dagger_{\boldsymbol{r},\uparrow}\hat{d}_{\boldsymbol{r}+a_0\hat{x},\downarrow}\rangle - \frac{\lambda^*_{x,\uparrow\downarrow}}{4}e^{\mathrm{i}\frac{\phi}{2}}\langle\hat{d}^\dagger_{\boldsymbol{r}+a_0\hat{x},\downarrow}\hat{c}_{\boldsymbol{r},\uparrow}\rangle\right.$$
$$\left. + \frac{\lambda_{x,\downarrow\uparrow}}{4}e^{-\mathrm{i}\frac{\phi}{2}}\langle\hat{c}^\dagger_{\boldsymbol{r},\downarrow}\hat{d}_{\boldsymbol{r}+a_0\hat{x},\uparrow}\rangle - \frac{\lambda^*_{x,\downarrow\uparrow}}{4}e^{\mathrm{i}\frac{\phi}{2}}\langle\hat{d}^\dagger_{\boldsymbol{r}+a_0\hat{x},\uparrow}\hat{c}_{\boldsymbol{r},\downarrow}\rangle\right]\Bigg). \tag{A11}$$

This quantity is computed using normal propagators between the sites in the X_R layer and sites in the first superconducting layer of the R lead. As $\Delta_0 \neq 0$, the calculation of the required propagators requires to work in the Nambu space since the equations of motion for normal and anomalous propagators are coupled. We write all the coupled equations using the standard method of Ref. 44 and obtain the normal propagators $\boldsymbol{G}^{r(a)}_{\boldsymbol{r}\sigma,\boldsymbol{r}'\sigma'}(\varepsilon)$.

c. Density of states and spin and current densities

After solving the equations of motion for the propagators, all the densities are obtained from[44]

$$\langle\hat{\xi}^\dagger_{\boldsymbol{r}',\sigma'}\hat{\xi}_{\boldsymbol{r},\sigma}\rangle = \int_{-\infty}^{\infty}\rho_{\boldsymbol{r}\sigma,\boldsymbol{r}'\sigma'}(\varepsilon)f_0(\varepsilon)\,d\varepsilon\,, \tag{A12a}$$

$$\rho_{\boldsymbol{r}\sigma,\boldsymbol{r}'\sigma'}(\varepsilon) \equiv \frac{\mathrm{i}}{2\pi}\left[\boldsymbol{G}^r_{\boldsymbol{r}\sigma,\boldsymbol{r}'\sigma'}(\varepsilon) - \boldsymbol{G}^a_{\boldsymbol{r}\sigma,\boldsymbol{r}'\sigma'}(\varepsilon)\right], \tag{A12b}$$

where the fermionic operators $\hat{\xi}$ are type $\hat{c}$, or $\hat{d}$ according to the region in which they operate.

When only the integrated quantity is important, for instance when studying the total Josephson current as a function of an external parameter, the integral in Eq. (A12a) can be computed in the complex plane by using the residue theorem. In this case, the number of integration points required for convergence is reduced by a factor of ten as we avoid the problem of integrating the chain of Dirac δs found in the real axis for $|\varepsilon| < \Delta_0$.

[1] R. Winkler, *Spin-Orbit Coupling Effects in Two-Dimensional Electron and Hole Systems* (Springer, Berlin, 2003).
[2] I. Žutić, J. Fabian, and S. Das Sarma, Rev. Mod. Phys. **76**, 323 (2004).
[3] *Semiconductor Spintronics and Quantum Computation*, edited by D. Awschalom, N. Samarth, and D. Loss (Springer, New York, 2002).
[4] D. Awschalom, Physics **2**, 50 (2009).
[5] M. König, S. Wiedmann, C. Brüne, A. Roth, H. Buhmann, L. W. Molenkamp, X. L. Qi, and S. C. Zhang, Science **318**, 766 (2007).
[6] C. L. Kane and E. J. Mele, Phys. Rev. Lett. **95**, 146802 (2005).
[7] X.-L. Qi and S.-C. Zhang, Rev. Mod. Phys. **83**, 1057 (2011).
[8] M. Franz, Physics **3**, 24 (2010).
[9] R. F. Service, Science **332**, 193 (2011).
[10] L. Fu and C. L. Kane, Phys. Rev. Lett. **100**, 096407 (2008).
[11] J. D. Sau, R. M. Lutchyn, S. Tewari, and S. Das Sarma, Phys. Rev. Lett. **104**, 040502 (2010); J. Alicea, Phys. Rev. B **81**, 125318 (2010); Y. Oreg, G. Refael, and F. von Oppen, Phys. Rev. Lett. **105**, 177002 (2010).
[12] E. V. Bezuglyi, A. S. Rozhavsky, I. D. Vagner, and P. Wyder, Phys. Rev. B **66**, 052508 (2002).
[13] I. Krive, S. Kulinich, R. Shekhter, and M. Jonson, Low Temp. Phys. **30**, 554 (2004).
[14] I. V. Krive, A. M. Kadigrobov, R. I. Shekhter, and M. Jonson, Phys. Rev. B **71**, 214516 (2005).
[15] O. V. Dimitrova and M. V. Feigel'Man, J. Exp. Theor. Phys. **102**, 652 (2006).
[16] L. Dell'Anna, A. Zazunov, R. Egger, and T. Martin, Phys. Rev. B **75**, 085305 (2007).
[17] B. Béri, J. H. Bardarson, and C. W. J. Beenakker, Phys. Rev. B **77**, 045311 (2008).
[18] A. Zazunov, R. Egger, T. Jonckheere, and T. Martin, Phys. Rev. Lett. **103**, 147004 (2009).
[19] A. G. Mal'shukov, S. Sadjina, and A. Brataas, Phys. Rev. B **81**, 060502 (2010); A. G. Mal'shukov and C. S. Chu, *ibid.* **84**, 054520 (2011).
[20] J. A. M. van Ostaay, A. R. Akhmerov, and C. W. J. Beenakker, Phys. Rev. B **83**, 195441 (2011).
[21] H. Takayanagi, T. Akazaki, and J. Nitta, Phys. Rev. Lett. **75**, 3533 (1995); H. Takayanagi and T. Akazaki, Phys. Rev. B **52**, R8633 (1995).
[22] A. A. Reynoso, G. Usaj, C. A. Balseiro, D. Feinberg, and M. Avignon, Phys. Rev. Lett. **101**, 107001 (2008).
[23] A. A. Golubov, M. Y. Kupriyanov, and E. Il'ichev, Rev. Mod. Phys. **76**, 411 (2004).
[24] A. I. Buzdin, Rev. Mod. Phys. **77**, 935 (2005).

[25]I. O. Kulik, Sov. Phys. JETP **30**, 944 (1969).
[26]J.-F. Liu and K. S. Chan, Phys. Rev. B **82**, 125305 (2010).
[27]I. Margaris, V. Paltoglou, and N. Flytzanis, J. Phys.: Condens. Matter **22**, 445701 (2010).
[28]M. Eto, T. Hayashi, and Y. Kurotani, J. Phys. Soc. Jpn. **74**, 1934 (2005).
[29]P. G. Silvestrov and E. G. Mishchenko, Phys. Rev. B **74**, 165301 (2006).
[30]A. Reynoso, G. Usaj, and C. A. Balseiro, Physica B **384**, 28 (2006). Phys. Rev. B **75**, 085321 (2007).
[31]J. J. Krich and B. I. Halperin, Phys. Rev. B **78**, 035338 (2008).
[32]A. T. Ngo, P. Debray, and S. E. Ulloa, Phys. Rev. B **81**, 115328 (2010).
[33]Andreev states are bound states, however, through them, Cooper pairs are transferred between superconductors. In this work, we call *velocity* of an Andreev state the velocity of the associated Cooper pair being transferred [see Eq. (13) and Fig. 3].
[34]A. A. Reynoso, Universidad Nacional de Cuyo, Instituto Balseiro, Bariloche, Argentina, 2009.
[35]J. C. Cuevas, A. Martín-Rodero, and A. LevyYeyati, Phys. Rev. B **54**, 7366 (1996).
[36]H. M. Pastawski and E. Medina, Rev. Mex. Fisica 47s1, 1 (2001).
[37]P. G. de Gennes, *Superconductivity of Metals and Alloys* (Benjamin, New York, 1966).
[38]T. Matsuyama, C.-M. Hu, D. Grundler, G. Meier, and U. Merkt, Phys. Rev. B **65**, 155322 (2002).
[39]G. E. Blonder, M. Tinkham, and T. M. Klapwijk, Phys. Rev. B **25**, 4515 (1982).
[40]E. Merzbacher, *Quantum Mechanics* (Wiley, New York, 1998).
[41]J. Nitta, T. Akazaki, H. Takayanagi, and T. Enoki, Phys. Rev. Lett. **78**, 1335 (1997).
[42]F. J. Dyson, J. Math. Phys. **3**, 1199 (1962).
[43]B. D. Josephson, Phys. Lett. **1**, 251 (1962).
[44]D. N. Zubarev, Usp. Fiz. Nauk **70**, 71 (1960) [Sov. Phys. Usp. **3**, 320 (1960)].
[45]A. C. Potter and P. A. Lee, Phys. Rev. Lett. **105**, 227003 (2010).
[46]A. F. Andreev, Sov. Phys. JETP **19**, 1228 (1964).
[47]P. F. Bagwell, Phys. Rev. B **46**, 12573 (1992).
[48]A. Furusaki, H. Takayanagi, and M. Tsukada, Phys. Rev. Lett. **67**, 132 (1991); Phys. Rev. B **45**, 10563 (1992).
[49]M. Ebel, C. Busch, U. Merkt, M. Grajcar, T. Plecenik, and E. Ilichev, Phys. Rev. B **71**, 052506 (2005).
[50]I. L. Aleiner and V. I. Fal'ko, Phys. Rev. Lett. **87**, 256801 (2001).
[51]M. Kjaergaard, K. Wölms, and K. Flensberg, Phys. Rev. B **85**, 020503 (2012).
[52]Except for the special case of identical linear-Dresselhaus and Rashba strengths for which some in-plane directions can also lead to a symmetry blockade of the current for $\phi = 0$.
[53]D. D. Kuhn, N. M. Chtchelkatchev, G. B. Lesovik, and G. Blatter, Phys. Rev. B **63**, 054520 (2001).
[54]C. W. J. Beenakker and H. van Houten, in *Single-Electron Tunneling and Mesoscopic Devices*, edited by H. Koch and H. Lübbig (Springer, Berlin, 1992), pp. 175–179; G. Wendin and V. S. Shumeiko, Superlattices Microstruct. **20**, 569 (1996).
[55]As shown in Fig. 4 of Ref. 22.
[56]D. K. Ferry and S. M. Goodnick, *Transport in Nanostructures* (Cambridge University Press, New York, 1997).
[57]T. Ando, Phys. Rev. B **44**, 8017 (1991).